TU Delft

Climate-analogy mapping as a tool to develop a temporally-adaptive hydrological model of the Meuse basin for more reliable predictions under change

E.J. van Noppen
MSc Thesis
08 April 2022

Delft University of Technology
Faculty of Civil Engineering & Geosciences
Water Management - Hydrology

Climate-analogy mapping as a tool to develop a temporally-adaptive hydrological model of the Meuse basin for more reliable predictions under change.

Elisabeth Jannigje van Noppen
5154235

to obtain the degree of Master of Science
at the Delft University of Technology

Thesis Committee:
Dr. Markus Hrachowitz - Delft University of Technology
Dr. ir. Oswaldo Morales Napoles - Delft University of Technology
Dr. ir. Ruud van der Ent - Delft University of Technology
Eric Sprokkereef - Rijkwaterstaat
Jasper Stam - Rijkwaterstaat
Laurène Bouaziz - Deltares

Faculty of Civil Engineering & Geosciences
Water Management - Hydrology
Netherlands

De Boucle-de-Monthermé in de Franse Ardennen

Summary

The root-zone storage capacity (S_r) represents the amount of water that is stored in the soil pore volume, which is accessible for vegetation to extract water for transpiration. S_r has a critical function in the partitioning of water fluxes, making it a key component in hydrological models (Savenije & Hrachowitz, 2017). There are different ways to compute the root-zone storage capacity. For example, the water balance method, which assumes that the root-zone storage capacity is derived from the maximum annual water deficits that results from the difference between the cumulative daily precipitation and transpiration (e.g. Gao et al., 2014; Nijzink et al., 2016). In hydrological models it is common practice to estimate the root-zone storage capacity by calibrating the parameter with the use of observed historical climate conditions. The model then assumes that the parameters do not change when the model is forced with future climate projection data (e.g. Parajka et al., 2016; Marx et al., 2018). This approach assumes that the parameter values are static in time. However, this is not a plausible assumption for long term predictions as it neglects any hydrological changes in the system. Recent studies have shown the importance of time-dynamic root-zone storage capacities in hydrological models to predict the future hydrological response of the system (Gao et al., 2014; Bouaziz et al., 2021). The current methods to compute the root-zone storage capacity contain a number of uncertainties, especially when we want to quantify the impact that the changing climate will have on future S_r values.

The aim of this research is (1) to propose a regression relationship using climate analogy, to estimate the time-dynamic root-zone storage capacity for the Meuse basin and (2) to quantify the impact of this time-dynamic root-zone storage capacity on the change in hydrological response under future climate conditions. The time-dynamic root-zone storage capacity is created by estimating the root-zone storage capacity for simulated historical and 2K climate data.

Previous studies have shown that the root-zone storage capacity can be associated with different catchment characteristics, like leaf cover, seasonality timing index, runoff-coefficient and aridity index (de Boer-Euser et al., 2019; van Voorst, 2020; Gao et al., 2014). In this study we propose a regression relationship between the root-zone storage capacity and a selection of catchment descriptors. This relationship has been derived based on climate analogy mapping. Climate analogy mapping is the practice of matching the expected future climate at one location with the current climate of another location (Fitzpatrick & Dunn, 2019). This means that the root-zone storage capacities of the 2K Meuse catchments are matched to the root-zone storage capacities of current catchments with similar catchment descriptors.

This study uses four data sets for the analysis, CAMELS-USA, CAMELS-GB, LamaH for Central Europe, and observed historical E-OBS data for the Meuse catchments. Catchments with little human influence and less then 10% annual snowfall were selected for the analysis. 27 catchment descriptors have been calculated for each of the selected catchments. These descriptors describe the characteristics of a catchment by climatic, soil, land-use and topography. Additionally, the root-zone storage capacity for each of the selected catchments has been computed using the water-balance

method. Multi-Linear Regression (MLR) analysis has been applied using the computed root-zone storage capacities and the catchment descriptors. The regression relationship that is derived states that the root-zone storage capacity can be estimated based on the Holdridge Aridity Index (HAI), phase shift of precipitation (s_P), seasonal amplitude for the potential evaporation (δ_E) and sand fraction (sand_frac) (Equation 1).

$$S_r = \beta_0 + \beta_{HAI} * HAI + \beta_{s_P} * s_P + \beta_{\delta_E} * \delta_E + \beta_{sand_{frac}} * sand_{frac} \quad (1)$$

The regression relationship has been used to estimate the root-zone storage capacity of the Meuse catchments for the simulated historical climate data (Sr-Hist$_{\mathrm{RM}}$) and the simulated 2K climate data (Sr-2k$_{\mathrm{RM}}$). The root-zone storage capacity for the simulated historical climate data has also been computed with the water balance method (Sr-Hist$_{\mathrm{WB}}$). Comparing Sr-Hist$_{\mathrm{RM}}$ to Sr-Hist$_{\mathrm{WB}}$ gives a mean error of 25 mm, which indicates that the regression method has a significant error with the water balance method. Comparing Sr-Hist$_{\mathrm{RM}}$ to Sr-2k$_{\mathrm{RM}}$ indicates that the simulated 2K climate data results in an increase of the root-zone storage capacity by 11.8%.

The Wflow_FLEX-Topo model has been used to quantify the impact of a time-dynamic root-zone storage capacity. Three different model scenarios have been considered for the Meuse catchments. Each scenario consists of a run that models the historical hydrological response, which is forced using the simulated historical climate data, and a run that represents the 2K hydrological response which is forced using the simulated 2K climate data. The difference in hydrological response between the two model runs has been determined for each model scenario. The three model scenarios are: (1) The benchmark for the water balance method, this scenario uses the Sr-Hist$_{\mathrm{WB}}$ for both the historical and 2K run of the model, (2) The benchmark for the regression relationship, this scenario uses the Sr-Hist$_{\mathrm{RM}}$ for both the historical and 2K run of the model, and (3) The dynamic regression relationship, which uses the Sr-Hist$_{\mathrm{RM}}$ for the historical run and Sr-2K$_{\mathrm{RM}}$ for the 2K run of the model.

Both benchmark models use a static root-zone storage capacity, the only difference between the scenarios is the method with which the root-zone storage capacity is estimated. By comparing the benchmark scenarios, we can quantify the impact of the regression relationship on the hydrological response of the system. The differences between the two scenarios in projected change of the streamflow, actual evaporation, root-zone moisture storage, and groundwater storage range between 0.2-1.12%, 0-1.5%, 0.03-1.1%, and 0.44-0.87%, respectively. The relatively small differences show that the regression method is in good agreement with the water balance method, making the benchmark scenario for the regression a realistic reference scenario with which the impact of the time-dynamic root-zone storage capacity can be identified.

Comparing the dynamic regression scenario to the regression benchmark scenario indicates that the implementation of the time-dynamic root-zone storage capacity results in changes in mean monthly hydrological response for the streamflow, actual evaporation, root-zone moisture storage, and groundwater storage with maximum -8.6%, +6.6%, +23.6%, and -4.8% respectively. These values indicate that the use of a time-dynamic root-zone storage capacity results in an increase of absolute evaporation during the summer months, while at the same time resulting in lower values for the streamflow and groundwater storage during the winter months. The root-zone storage capacity shows an increase throughout the whole year. In other words, the time-dynamic root-zone storage capacity has a significant impact on the seasonality of the change in the hydrological response.

To conclude the use of a time-dynamic root-zone storage capacity parameter has a large impact on the hydrological response of a system. The results of the regression relationship are promising and suggest that it might be a good way to estimate the root-zone storage capacity for climate projections in temperate climates. How-

ever, for the direct implementation of this relationship into hydrological models, a decrease in the error with the water balance would be favorable. Therefore, further research regarding the root-zone storage capacity might provide new insights and create a better understanding regarding the processes that influence the root-zone storage capacity.

Contents

List of Figures

List of Tables

Nomenclature

Abbreviations

HRU	Hydrological Response Unit
MAE	Mean absolute error
MAPE	Mean absolute percentage error
ME	Mean error
MLR	Multi-Linear Regression
PCA	Principal Component Analysis

Symbols

δ_E	Seasonal potential evaporation amplitude [-]
δ_P	Seasonal precipitation amplitude [-]
Δ_T	Seasonal temperature amplitude [°C]
AI	Aridity Index [-]
E_P	Potential evaporation [LT^{-1}]
E_T	Transpiration [LT^{-1}]
HAI	Holdridge Aridity Index [-]
hpd	High precipitation duration [T]
hpf	High precipitation frequency [T]
hpt	High precipitation timing [TT^{-1}]
is_{dur}	Interstorm duration [T]
lpd	Low precipitation duration [T]
lpf	Low precipitation frequency [T]
lpt	Low precipitation timing [TT^{-1}]
P	Precipitation [LT^{-1}]
Q	Streamflow [LT^{-1}]
s_d	Phase shift between temperature and precipitation [T]
s_E	Phase shift of the potential evaporation [T]
s_P	Phase shift of the precipitation [T]
S_r	Root-zone storage capacity [L]
s_T	Phase shift of the temperature [T]
S_D	Storage deficit [L]
SI	Seasonality Index [-]

Sr-2K$_{RM}$ Root-zone storage capacity estimated for the simulated 2K climate data using the regression relationship[L]

Sr-Hist$_{RM}$ Root-zone storage capacity estimated for the simulated historical climate data using the regression relationship[L]

Sr-Hist$_{WB}$ Root-zone storage capacity computed for the simulated historical climate data using the water balance method [L]

ST Seasonality Timing Index [-]

T Temperature [°C]

1 | Introduction

In order to survive dry periods it is assumed that vegetation naturally adapts to changing hydro-climatic conditions at the eco-system scale (e.g. Wang-Erlandsson et al., 2016; de Boer-Euser et al., 2016). A critical strategy for vegetation is the adaptation of its root-system. This strategy impacts the root-zone storage capacity (S_r) of the system, which represents the amount of water that is stored in the soil pore volume, that is accessible for vegetation to extract water for transpiration. The vegetation adapts its root-zone storage capacity to satisfy canopy water demand, creating a buffer to survive dry periods (Bouaziz et al., 2021; Gao et al., 2014). This sub-surface property is at the core of any hydrological system as it regulates the water storage release dynamics and in particular the partitioning of water into evaporative fluxes and drainage (Savenije & Hrachowitz, 2017).

The critical function of the root-zone storage capacity in the partitioning of water fluxes makes it a key component in hydrological models. It is common practice for these models to estimate the root-zone storage capacity by calibrating the parameter with the use of observed historical climate conditions. The model then assumes that the parameters do not change when it is forced with future climate projection data (e.g. Parajka et al., 2016; Marx et al., 2018). By using present day model parameters for future predictions it is assumed that the properties of the hydrological system do not change over time. For near future projections this assumption seems plausible, as there are no fundamental changes to the hydrology. However, for long-term predictions, this assumption is in clear contrast with the notion that vegetation actively adapts its root-system. Moreover, it neglects the possible impact that climate change might have on vegetation species and land-use.

Different approaches can be used to quantify the value of the root-zone storage capacity on a catchment scale. The value can be determined based on field observations, as the product of root-depths or root-distributions and the pore water content between field capacity and permanent wilting point. This approach gives accurate values for the root-zone storage capacity, but can be difficult to apply on a catchment scale, as the required data is typically not available at a sufficient resolution (Hrachowitz et al., 2020). Another approach is to estimate the root-zone storage capacity with the use of a look-up table. The estimates are based on literature values of the mean biome rooting depth and soil texture data. This approach makes the root-zone storage capacity a function of land cover and soil type, thereby fully neglecting the impact of the climatic conditions (Wang-Erlandsson et al., 2016). Moreover, the root-zone storage capacity value can also be estimated by calibration of a hydrological model. The calibration approach uses hydrological observations from the precipitation, evaporation, and streamflow to determine the root-zone storage capacity. This method can be used at a catchment scale, however the resulting values are tied to the model for which the calibration has been used. Therefore, they are not necessarily comparable to measurable values in nature. They also tend to compensate for uncertainties in model structure and data (Wang-Erlandsson et al., 2016). Alternatively, increasing evidence has shown that the root-zone storage capacity at catchment-scale can be robustly and directly estimated using water balance data. The water balance method assumes that the root-zone storage capacity is derived from the maximum annual

water deficits that results from the difference between the cumulative daily precipitation and transpiration (Gao et al., 2014; Nijzink et al., 2016; de Boer-Euser et al., 2016; Wang-Erlandsson et al., 2016; Bouaziz et al., 2021; Hrachowitz et al., 2020).

These methods use different catchment characteristics to compute the root-zone storage capacity. The look-up approach bases the value on rooting depth and soil structure, while the calibration and water balance method use hydrological data. The relationship between the root-zone storage capacity and different catchment characteristics has been investigated in multiple studies. de Boer-Euser et al. (2019) showed that the root-zone storage capacity has a positive correlation with leaf cover, tree length, and biomass. On the other hand van Voorst (2020) concluded that the variance of S_r between catchments in Canada was mainly described by a combination of long-term average variables (aridity index and runoff coefficient) and by the coherence of seasonal and timing effects (seasonality timing index). Gao et al. (2014) also indicated that aridity index and seasonality index were positively correlated to the root-zone storage capacity.

Climate change causes the altering of the means and extremes of precipitation, evaporation, and streamflow rates of rivers (Milly et al., 2008). Climate analogy mapping is the practice of matching the expected future climate at one location with the current climate of another location. This technique can be used to visualize how the climate zones will shift over the Earth's surface as a result of climate change. Fitzpatrick & Dunn (2019) studied urban areas in North America. This study shows that the future climate of most urban areas match urban climates that are currently hundreds of kilometers away.

The fast changing climatic conditions make that stationarity is no longer a valid assumption. The predictions that are made by hydrological models that use static parameters are subjected to increasing uncertainties. Therefore, it is important to quantify the non-stationarity of relevant hydrological parameters, as a temporally-adaptive hydrological model will likely provide more reliable predictions under change. With better predictions of future hydrological responses, catastrophic events in the river system can be predicted and suitable measures can be created to prevent such events from happening in the future. For example, by building water retention areas or applying dyke reinforcements.

1.1 Problem statement

Multiple studies have described the importance of a non-stationary or time-dynamic root-zone storage capacity in hydrological models, to predict the future hydrological response of the system (Gao et al., 2014; Nijzink et al., 2016). Bouaziz et al. (2021) showed that the implementation of a time-dynamic root-zone storage capacity in a process-based hydrological model, for the Meuse basin, could strongly alter the predicted hydrological response to a 2K warming projection. Current methods result in a number of uncertainties when they are used to quantify the impact that the changing climate will have on the future S_r values. The methods are not suitable for catchment scale computations or their use is limited by the data that is needed for the computations. Each method contains a level of uncertainty, since there is no perfect method to determine the root-zone storage capacity.

1.2 Research objective

In this study we propose a new method to estimate the root-zone storage capacity by combining the fact that the root-zone storage capacity can be associated with a number of catchment characteristics with the principle of climate analogy. We assume that two catchments with the same characteristics will have the same root-zone

storage capacity. This means that knowing the future characteristics of a catchment makes it possible to determine the future root-zone storage capacity. To be able to quantify this analogy a regression relationship has been derived between the root-zone storage capacity and a selection of catchment characteristics. The objective of this study is (1) to propose a regression relationship using climate analogy to estimate the time-dynamic root-zone storage capacity for the Meuse basin, and (2) to quantify the impact of this time-dynamic storage capacity on the change in hydrological response under future climate change.

Since previous studies have suggested that the root-zone storage capacity can be correlated to different catchment characteristics (van Voorst, 2020; de Boer-Euser et al., 2019; Gao et al., 2014), we hypothesize that we can make reliable estimates of the root-zone storage capacity using a regression relationship with the use of catchment descriptors. Moreover, we hypothesize that the use of a time-dynamic root-zone storage capacity will change the hydrological response, by resulting in more pronounced seasonality changes under future conditions relative to current-day conditions.

This study will use large sample data sets containing catchments with a broad range of climate characteristics that are relatively close to the conditions of the current and future Meuse basin. The S_r value of these catchments has been computed with the water balance method. Additionally, for each catchment the values of 27 catchment descriptors were also computed. From this data a regression relationship has been derived by correlating the catchment descriptors to the root-zone storage capacity. Based on this regression relationship, the root-zone storage capacity is estimated for simulated historical and 2K climate data of the Meuse basin. These two S_r estimates create a time-dynamic root-zone storage capacity. The Wflow_FLEX-Topo model has been used to quantify the impact of a time-dynamic root-zone storage capacity on the change in hydrological response.

2 | Study Area

This study is focused on the river basin of the Meuse, which is an important basin for flood forecasting in the Netherlands (de Boer, 2017). This chapter provides general information regarding this river basin.

The Meuse river basin in Northwest Europe has a basin area of approximately 36 000 km^2 covering parts of the Netherlands, Belgium, France, Germany, and Luxembourg (Figure 2.1a). The source of the river is found at the Langres Plateau in France from where the river travels approximately 925 km to its mouth at the Rhine-Meuse-Scheldt delta in the Netherlands. Approximately 60% of the river basin is used for agricultural purposes and 30% is forested. The elevation ranges between approximately 50 and 750 m across the river basin (Figure 2.1b) (de Wit, Peeters, et al., 2007).

The basin area can be divided into three major geological zones. The first zone is located South of Charleville-Mézières and is called the Lorraine Meuse. This part mainly consists of sedimentary Mesozoic rocks. The area is characterized by hilly landscapes with wide floodplains through which the Meuse flows. The second zone is called the Ardennes Meuse. Here the river transects the paleozoic rock of the Ardennes Massif. This part is characterized by narrow, steep valleys. The last geological zone consists of the Dutch and Flemmish lowlands. The area is made up of Cenozoic unconsolidated rocks and can be characterized by wide floodplains and a low river gradient (de Wit, Peeters, et al., 2007).

The Meuse is located in a zone with temperate climate conditions. This climate zone is characterized by frequent weather variations (Pfister et al., 2004). The streamflow of the rain-fed river experiences strong seasonality. The river has high streamflow during the winter months and low streamflow during the summer months. The average summer streamflow of the Meuse is approximately one quarter of the average winter streamflow (de Wit, van den Hurk, et al., 2007). Since the precipitation remains relatively constant throughout the year, the seasonality in the streamflow represents the fluctuation in potential evaporation. High potential evaporation in the summer, results in relatively low streamflow, while low potential evaporation in the winter results in high streamflow. The snow impact in the basin area is generally small, however it can be of significant importance in specific events (de Boer, 2017). The mean annual precipitation, potential evaporation, and streamflow of the Meuse basin are approximately 968 mm yr^{-1}, 593 mm yr^{-1}, and 397 mm yr^{-1} respectively. These values are computed using the observed historical E-OBS climate data and the streamflow data (Section 3.1).

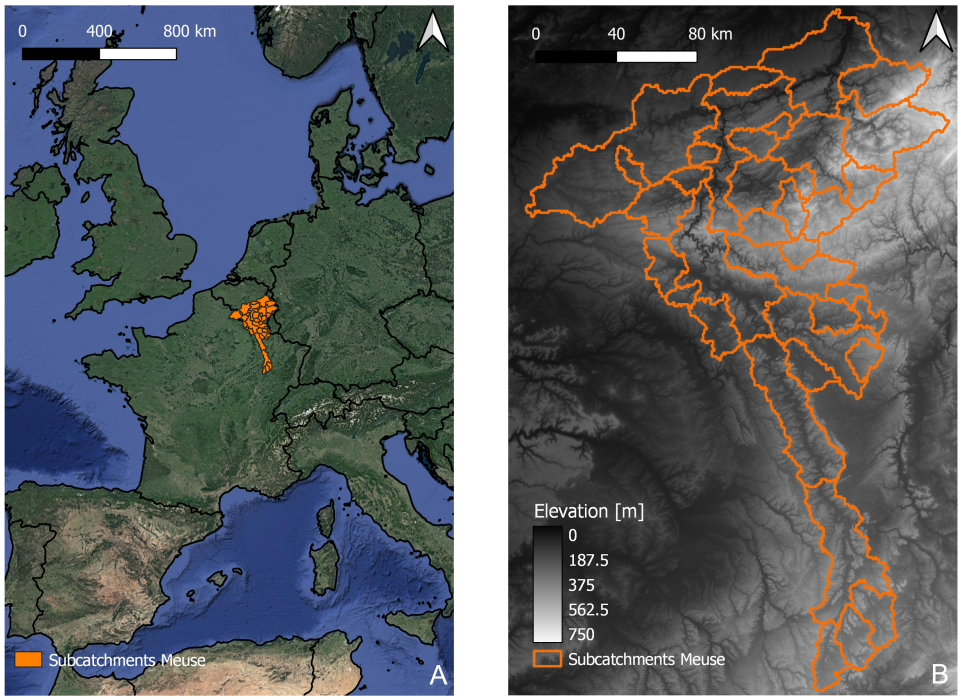

Figure 2.1: (a) The Location of the Meuse basin in Northwest Europe. (b) The elevation range in the basin and the location of the 35 catchments of the Meuse basin

3 | Data sources

The data sets that are used in this study can be divided into two groups. The first group contains the data sets that describe the historical and future climate conditions of the Meuse basin. The second group consists of large sample catchment data sets. This chapter describes the data sources and the corrections that were made.

3.1 Meuse Data

The Meuse basin is divided into 35 catchments (Figure 2.1b). This section describes the source of three meteo-hydrological data sets for the Meuse, followed by the streamflow data and additional catchment data that have been used in this research.

3.1.1 Observed historical E-OBS climate data

The E-OBS data set (v20.0e) is based on the station data collated by the European Climate Assessment Dataset (ECA&D) initiative. It contains daily gridded observation data for the precipitation, temperature, and sea level pressure in Europe. The data is provided at a 25 km^2 resolution for the period between 1980 and 2018 (Cornes et al., 2018). Bouaziz et al. (2021) has pre-processed the data for the Meuse catchments by using a digital elevation model and a fixed lapse rate of 0.0065 °C m^{-1} to downscale the temperature. Additionally, a monthly bias-correction factor has been applied improving the consistency between the precipitation estimates of the E-OBS dataset and the local precipitation data that was provided by the Service Public de Wallonie, because the difference between the two data sets exceeded 20% in the center of the Meuse catchment. Lastly, the potential evaporation has been estimated using the Makkink formula (Hooghart & Lablans, 1988).

3.1.2 Simulated Climate data

The Royal Netherlands Meteorological Institute (KNMI) provides two simulations for the climatic conditions of the Meuse catchments, a historical climate simulation for the period 1979-2018 and a 2K global warming simulation. These simulations have been generated at 12 km x 12 km resolution, with the regional climate model KNMI-RACMO2 (van Meijgaard et al., 2008). The KNMI-RACMO2 model uses initial- and lateral boundary conditions based on which the climate conditions are simulated. For the historical climate simulation the initial- and lateral boundary conditions are provided by the ERA5 reanalysis data (Hersbach et al., 2020). To generate high-resolution climate change information the 2K global warming simulation uses an alternative method, so-called pseudo-global warming (PSG) (Schär et al., 1996). This method re-simulates the historical period, with perturbations to the initial and boundary conditions that are provided by the ERA5. These perturbations mimic the change in the mean climate state under the conditions that occur with a globally 2K warmer world. These perturbations have been derived from a large initial condition Global Climate Model (GCM) ensemble (Aalbers et al., 2018). Aalbers et al. (2019) provides a full description of the simulation data sets.

3.1.3 Streamflow

The streamflow data covers the period 2005 to 2017 for the 35 catchments that are nested within the Meuse basin in the area upstream of Borgharen. Borgharen is located downstream of a river stretch at the border between Belgium and the Netherlands where a number of canals branch off. The total streamflow at Borgharen is a constructed time series, which sums the observed streamflow of the Meuse at St Pieter with the streamflow of the Albert Canal at Kanne, before part of it is extracted in the Albert Canal (Bouaziz et al., 2021; de Wit, Van Den Hurk, et al., 2007).

3.1.4 Catchment attributes

Besides the hydro-meteorological conditions of the Meuse catchments, we used additional data sets to obtain information regarding topography, land-use, and soil characteristics of the Meuse basin. MERIT Hydro data (Yamazaki et al., 2019) has been used to determine the slope and land elevation. The land-use characteristics of the catchments have been determined based on CORINE Land Cover data (Agency, 2020). Lastly, the soil properties have been selected from the SoilGrids at a resolution of 250 m (Hengl et al., 2017).

3.2 Large Sample Data sets

We also used three different large sample data sets, namely CAMELS-USA, CAMELS-GB, and LamaH for Central Europe. CAMELS stands for Catchment Attributes and Meteorology for Large-sample Studies and LamaH stands for Large-sample Data for Hydrology. In this section the origin of the data sets will be described as well as the corrections that have been applied.

3.2.1 CAMELS-USA

The CAMELS data set for the contiguous United States (CONUS) is a combination of the hydro-meteorological time series provided by Newman et al. (2015) and the catchment attributes provided by Addor et al. (2017). The catchments are a selection of the Geospatial Attributes of Gages for Evaluating Streamflow (GAGES-II) from the United States Geology Survey (USGS) of 2011 (Falcone et al., 2010; Falcone, 2011). The gages that have been selected are marked as HCDN-2009 (Lins, 2012), meaning that they meet the following criteria: 1) the gages were active as of 2009 and have complete flow data for at least 20 years in the period between 1990 and 2009, 2) the gage is a GAGES-II reference gage, 3) The National Land Cover Database (NLCD-2011) measures less than 5% imperviousness (Jin et al., 2013), and 4) they passed a manual survey of human impacts in the basin by local Water Science Center evaluators (Falcone et al., 2010). These gages have been used as the starting point for the CAMELS data set, as they should best represent natural flow conditions. After initial processing and data availability requirements, the 671 remaining catchments were combined for the CAMELS-USA data set (Newman et al., 2015). The location of the catchments are shown in Figure 3.1b.

The data set provides meteorological forcing and observed discharge data for the period between 1981 and 2008. The forcing includes three data sets: NLDAS, Maurer, and Daymet. In this study the Daymet data set has been selected, since this daily-gridded data has the highest spatial resolution (1 x 1 km). The data is derived from daily observations of temperature and precipitation. In this study the following variables have been used from the data: daily maximum and minimum temperature, precipitation, shortwave downward radiation, and day length. These daily values are estimated with the use of an iterative method. The method is dependent on local station density as well as on the spatial convolution of a truncated Gaussian filter for station interpolation. To estimate the short-wave incoming radiation, the

Mountain Climate Simulator (MT-CLIM) has been used. The potential evaporation has been estimated using the Priestly-Taylor equation. The observed discharge data has been obtained from the USGS Water information System server for the period, 1980-2010. (Newman et al., 2015). In this study, the choice was made to use the data provided for the period 1 October 1989 to 30 September 2009 to describe the conditions within the catchments. This is the same time period that has been used for the computations of the climatic indices, due to the proportion of missing daily discharge measurements in the years before and after this period (Addor et al., 2017).

The CAMELS-USA data also provides additional catchment attributes, that are derived from different sources. Topography and location, hydrological signatures, and forest fraction are all extracted from the USGS data. The climatic indices have been derived with the use of the Daymet data set (Newman et al., 2015; Addor et al., 2017) and the soil characteristics have been obtained from Miller & White (1998).

For a full description of the data set the reader is directed to (Newman et al., 2015; Addor et al., 2017).

3.2.2 CAMELS-GB

The CAMELS-GB data set consists of 671 catchments across Great-Britain (Figure 3.1a). The catchments have been selected from the UK National River Flow Archive (NRFA) Service Level Agreement (SLA) Network. This network contains stations that are selected based on a number of criteria, including the hydrometric performance, representativeness of the catchment, length of record, and degree of artificial disturbance to the natural flow regime (Dixon et al., 2013; HANNAFORD, 2004). They have also been subjected to an additional level of validation from the NRFA (Muchan & Dixon, 2014), focused on the credibility of flows in the extreme ranges and the need to maintain sensibly complete time series. The resulting stations provide good-quality data for long time series. The daily streamflow data has been obtained from these stations (Coxon et al., 2020). Daily meteorological time series are provided covering the period between October 1st 1961 to September 30th 2015. In this study the following variables have been used from these time series: precipitation, temperature, and incoming short-wave radiation. The daily precipitation has been obtained from the CEH Gridded Estimates of Areal Rainfall dataset (CEH-GEAR) (Keller et al., 2015; Tanguy et al., 2016). The data set contains gridded estimates at a resolution of 1 km^2. The data has been derived with the use of natural neighbour interpolation of quality controlled, observed precipitation from the Met Office UK rain gauge network. The temperature and incoming shortwave radiation have been obtained from the Climate Hydrology and Ecology research Support System meteorology data set (CHESS-met) (E. Robinson et al., 2017). This data set consists of daily gridded estimates at a resolution of 1 km^2. The data has been derived from the 40 km gridded dataset MORECS, which has been derived by interpolating daily station data (Hough & Jones, 1997; Thomson et al., 1981) The temperature for the CAMELS-GB data has been directly downscaled from MORECS, while the incoming short-wave radiation has been calculated from the downscaled temperature, vapour pressure, and sunshine hours (E. L. Robinson et al., 2017). Potential evaporation has been estimated with the Penman-Monteith equation for FAO-defined well-watered grass (Allen et al., 1998). (Coxon et al., 2020).

This data set also provides each catchment with a number of catchment attributes (Coxon et al., 2020). The topographic attributes have been extracted from the UK National River Flow Archive using the NRFA, API, and the CEH's Integrated Hydrological Digital Terrain Model (Morris et al., 1990). The UK Centre for Ecology & Hydrology has produced the UK Land Cover Map (2015) that has been used to determine the land cover attributes of the catchments (Rowland et al., 2017). The soil attributes have been derived from the European Soil Database Derived Data product (Hiederer, 2013) and the modelled depth to bedrock global product (Pelletier et al.,

2016).

For a full description of the data set the reader is directed to (Coxon et al., 2020).

3.2.3 LamaH Central Europe

The LamaH data set for Central Europe consists of 859 catchments, which are spread out over 9 different countries, namely Austria, Germany, Czech Republic, Switzerland, Slovakia, Italy, Liechtenstein, Slovenia, and Hungary (Figure 3.1c). The data set contains meteorological and streamflow data. The meteorological data has been derived from the ERA5-Land data set with global coverage (Muñoz-Sabater et al., 2021). Gap-free time series have been obtained with daily resolution for 15 meteorological parameters in the period between October 1st 1989 and September 30th 2009. The ERA5-Land has a spacial resolution of 0.1 arc degrees. The observations are indirectly implemented via the assimilated atmospheric fields of ERA5 (Hennermann & Guillory, 2020; Yang & Giusti, 2020). The potential evaporation has been estimated using the Penman-Monteith equation for FAO-defined well-watered grass (Allen et al., 1998). The streamflow data has been derived from daily and hourly time series for 882 gauges, located in Austria, Germany, Switzerland, and Czech Republic. The data was provided by the Hydrographic Central Bureau of Austria (HZB, 2020), the hydrographical services of the German federal states Bavaria (GKD, 2020) and Baden-Württemberg (LUBW, 2020), hydrological office of Switzerland (BAFU, 2020), and the Czech Hydrometeorological Institute (CHMI, 2020). The time series have been derived from rating curves. The streamflow time series has been limited to the period 1981 to 2017, since the ERA5-Land forcings start in 1981 and 2017 is the last year for which the streamflow data from Austria was quality-controlled. When utilizing the data set, it is important to check the data availability, since not all institutes covered the same time period. (Klingler et al., 2021).

This data set includes several catchment attributes. Topographical indices have been derived using the Shuttle Radar Topography Mission digital elevation data, which is provided by NASA JPL at a resolution of approximately 30 m (Farr et al., 2007). The land cover attributes have been based on the CORINE Land Cover (CLC) 2012 raster with a grid-size of 100 m. The soil attributes have been derived from the European Soil Database Derived Data product (Hiederer, 2013).

For a full description of the data set the reader is directed to (Klingler et al., 2021).

3.2.4 Data Correction

The potential evaporation has been estimated with different formulas in the data sets. CAMELS-USA used the Priestly-Taylor equation while both the CAMELS-GB and LamaH data set used the Penman-Monteith equation for FAO-defined well-watered grass. The observed historical E-OBS data set used the Makkink equation to estimate the potential evaporation for the Meuse catchments. The different equations result in different values for the potential evaporation. In order to create more consistency between the data sets, an attempt has been made to use one method for all the data sets. Considering the fewer meteorological variables available in the observed historical E-OBS data set, we decided to compute the potential evaporation with the Makkink equation for the catchments of the large sample data sets. The Makkink equation uses the mean daily temperature and shortwave incoming radiation (Hooghart & Lablans, 1988).

For the CAMELS-USA data set the mean daily temperature is provided in degrees Celsius and the incident shortwave radiation flux density is provided in [W m^{-2}]. The radiation has been multiplied by the daily number of sunshine hours, to obtain the incoming shortwave radiation in [J $m^{-2}day^{-1}$] (Hiemstra & Sluiter, 2011). Appendix A provides the Makkink equation that has been applied to obtain the potential

evaporation.

For the CAMELS-GB data set the mean daily temperature is provided in degrees Celsius and the shortwave incoming radiation in [W m^{-2}]. Since this data did not contain daily sunshine hours, a variation of the Makkink equation has been used. Appendix A provides the Makkink equation that has been applied to obtain the potential evaporation.

The LamaH data set provides the temperature in degrees Celsius, however no suitable parameter for the shortwave incoming radiation has been provided. This makes it difficult to estimate the potential evaporation using the Makkink equation. Instead the potential evaporation estimates provided by the data set have been used in this study.

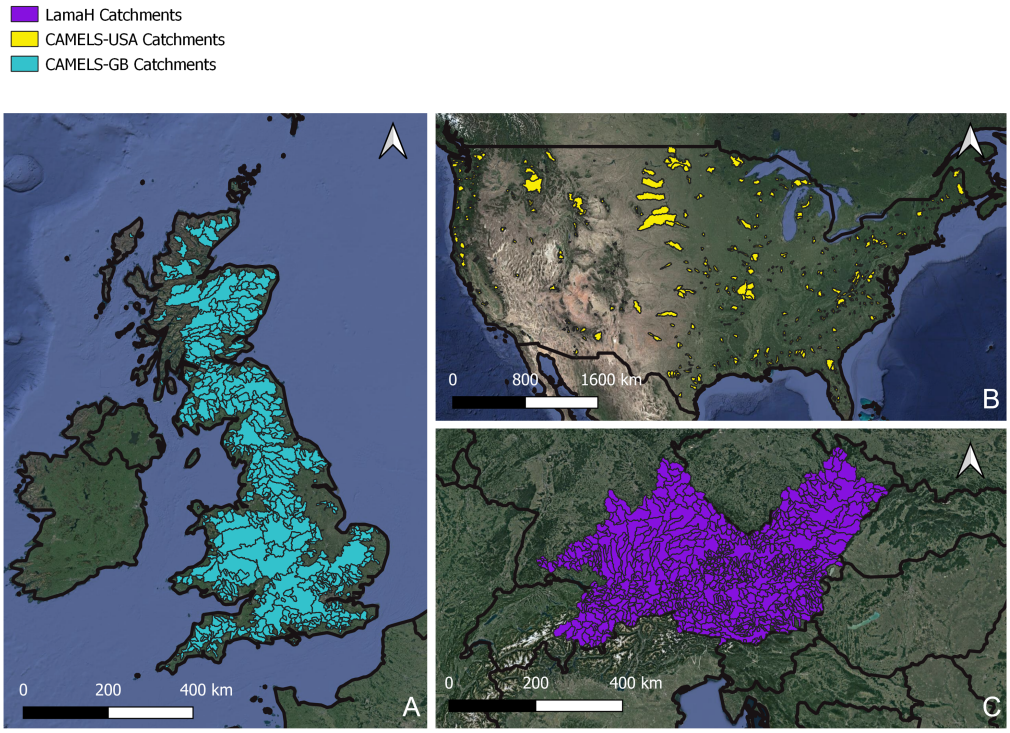

Figure 3.1: The locations of the catchments that are provided by (a) CAMELS-GB, (b) CAMELS-USA, and (c) LamaH of Central Europe.

4 | Methodology

This chapter provides a description of the different methods and strategies that have been used in this study. An overview of the methodology is shown in Figure 4.1. The chapter starts by discussing the water balance method for computing the root-zone storage capacity (Section 4.1), after which we discuss the regression approach that is based on climate analogy (Section 4.2). In Section 4.3 we discuss the Wflow_FLEX-Topo model and the way in which it is used to determine the impact of the dynamic root-zone storage capacity on the hydrological response. The entire approach of this study has been coded in Python. Appendix B provides an overview of the most relevant scripts that have been used.

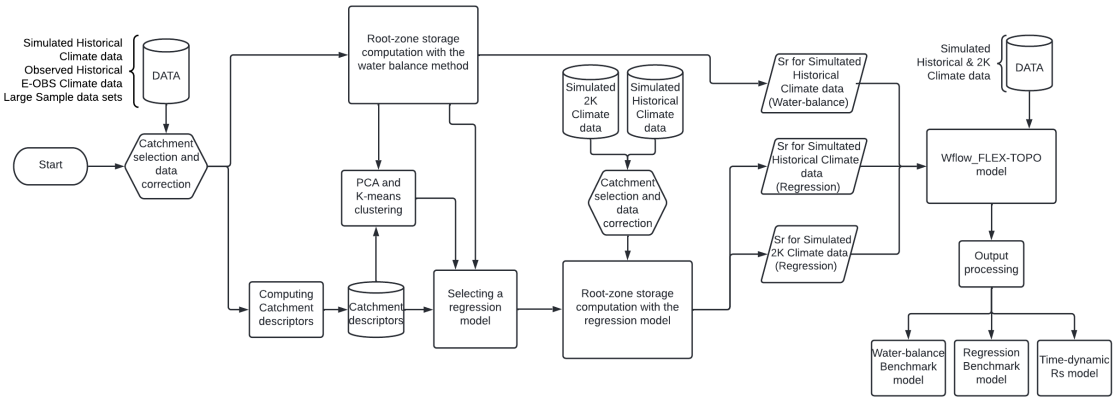

Figure 4.1: Flow diagram of the Methodology.

4.1 The water balance method

The root-zone storage capacity represents the amount of water that is stored in the soil pore volume, which is accessible for vegetation to extract water for transpiration. The vegetation and the hydrological system act in co-evolutionary way, to reach an equilibrium between the canopy water demand and the water availability in the system. The water balance method assumes that this equilibrium is maintained by the vegetation adapting its root-zone storage capacity, in order to create a large enough buffer to overcome a drought of a certain return period (Gao et al., 2014). The method assumes that the catchment-scale root-zone storage capacity can be derived from the maximum annual water deficits that results from the difference between the cumulative daily precipitation and transpiration. Figure 4.1, shows how the water balance method is used in this study.

The long-term water balance (Equation 4.1) has been used to derive an expression

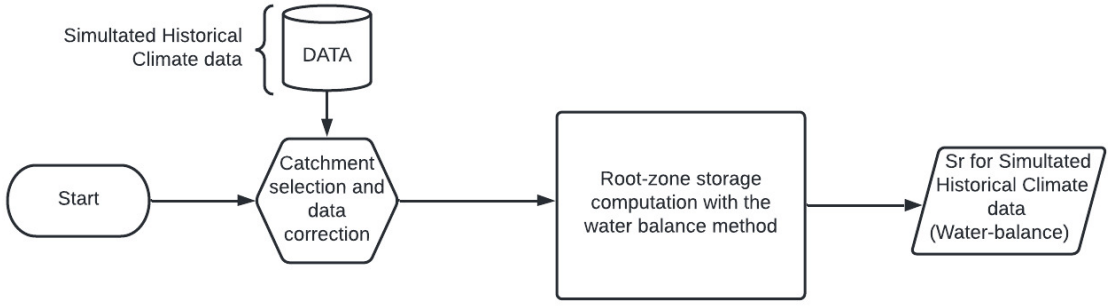

Figure 4.2: Flow diagram for the water balance method.

for the long-term mean transpiration ($\overline{E_T}$). For this study the changes in storage and inter-catchment groundwater flows are assumed to be zero. This results in the elimination of the storage factor from the water balance equation ($\frac{dS}{dt} = 0$). Moreover, interception and soil or built-surface evaporation have also been assumed negligible. These assumptions make it possible to rewrite the water balance and equate the long-term mean transpiration to the long-term mean evaporation (Equation 4.2).

$$\overline{P} - \overline{E_T} - \overline{Q} - \frac{dS}{dt} = 0 \tag{4.1}$$

$$\overline{E_T} = \overline{P} - \overline{Q} \tag{4.2}$$

The water balance approach requires daily precipitation (P) and transpiration (E_T) data. Daily precipitation observations are provided by the different data sets as described in Section 3. Currently there is no existing method that can be used to measure daily transpiration at the catchment scale. Therefore, transpiration data is not provided in any of the data sets. Estimations of the daily transpiration have been made by scaling the long-term mean transpiration with the ratio of the daily potential evaporation ($E_P(t)$) over the mean annual potential evaporation ($\overline{E_P}$) (Equation 4.3). Scaling the data with the use of the potential evaporation, retains the seasonality of transpiration without violating the long-term mean transpiration amounts.

$$E_T(t) = \frac{E_P(t)}{\overline{E_P}} \overline{E_T} \tag{4.3}$$

Based on the results of Equation 4.2 and 4.3, the cumulative deficit between the daily transpiration and precipitation can be calculated. During dry periods the transpiration will exceed the precipitation resulting in higher storage deficits. While periods with large amounts of precipitation will lead to a decrease of the storage deficit. The storage deficit is assumed to be zero at the start of the computation and should always be negative. The mathematical notation to compute the cumulative storage deficit is given in Equation 4.4.

$$S_D(t) = min(0, \int_{t_1}^{t_2} (P(t) - E_T(t))dt) \tag{4.4}$$

The annual maximum storage deficits have been fitted to the Gumbel extreme value distribution, to derive the root-zone storage capacity at the catchment scale for a certain return period. For this study the root-zone storage capacity has been determined using a return period of 20 years. This means that it is assumed that the root-systems of the vegetation have developed a buffer to survive droughts with a return period of 20 years.

The water balance method has been used to estimate the root-zone storage capacity for the Meuse catchments using the simulated historical climate data and the observed historical E-OBS data. Moreover, the method has also been used to compute the root-zone storage capacity for a selection of the Large sample data set catchments, this is discussed in the next section of this chapter.

4.2 The regression relationship

The aim of this study is to use climate analogy to estimate the time-dynamic root-zone storage capacity for the Meuse catchments. Climate analogy matches the expected future climate at one location with the current climate of another location. Assuming that the root-zone storage capacity can be estimated based on catchment characteristics, we state that catchments with the same catchment characteristics have the same root-zone storage capacity. The root-zone storage capacity of the future Meuse catchments can then be estimated by finding current locations with similar catchment characteristics. The relationship between the root-zone storage capacity and the catchment characteristics is derived with the use of Multi-Linear Regression analysis (MLR).

First we select catchments that are suitable to be part of the study based on several requirements, which are described in Section 4.2.1. This is followed by an explanation of the catchment descriptors that form the basis for the regression analysis (Section 4.2.2). To identify the existing patterns between the different catchment descriptors and the root-zone storage capacity, two different statistical procedures have been applied: Principal Component Analysis (PCA) and K-means Clustering (Section 4.2.3). Using the results from the statistical procedures, Multi-Linear Regression (MLR) analysis has been performed, resulting in an expression for the root-zone storage capacity based on a number of catchment descriptors (Section 4.2.4). Based on this relationship the root-zone storage capacity has been estimated for the simulated historical and 2K climate data of the Meuse catchments. Combining the S_r values of the simulated historical and 2K climate data, creates a time-dynamic root-zone storage capacity. Figure 4.5 provides a schematic overview of this section.

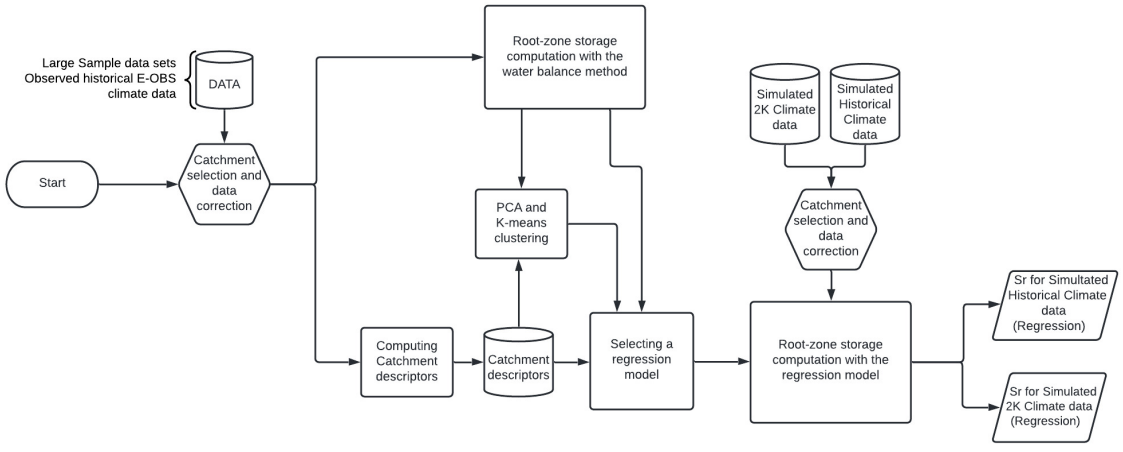

Figure 4.3: Flow diagram for the regression relationship.

4.2.1 Catchment Selection

The data sets that are discussed in the previous chapter contain a multitude of catchments. Not all of the catchments are suitable to be part of the regression relationship. Therefore, a selection has been made based on the following requirements. Firstly,

the catchment should have natural flow conditions. This means that the impact of human activities in the catchment should be minimal, as human activities can drastically alter the root-zone storage capacity resulting in unreliable model outcomes. Secondly, the catchments should experience little snowfall. Snowfall is a complex process as it has the ability to store water for a period of time, before it melts and transforms from a storage to a flux. The root-zone storage capacity in catchments with significant snowfall can be under- or overestimated due to this delay of water input (de Boer-Euser et al., 2019). This problem is eliminated by only selecting catchments with little snowfall. The snowfall is considered to be little when it makes up less than 10% of the annual precipitation. For each catchment this percentage has been calculated by dividing the annual precipitation on days with a negative temperature by the annual precipitation amount. The catchments that met these requirements have been processed and checked for data availability and reliability, which resulted in the elimination of some additional catchments.

4.2.2 Catchment descriptors

This section describes the different catchment descriptors. The descriptors have been selected based on recent studies focusing on the relationship between root-zone storage capacity and catchment characteristics. Additionally, each descriptor should be able to be calculated based on data provided by future climate projections. The catchment descriptors can be divided into two categories. The first category contains climatic descriptors and can be computed with meteorological data. The second category consist of landscape descriptors including topography, land-use, and soil characteristics. Table 4.1 gives an overview of all the catchment descriptors that are discussed.

Climatic descriptors

The climatic catchment descriptors have been computed for the selected catchments using the python scripts provided in Appendix B. For CAMELS-USA the calculations have been done with the time period between January 1st 1980 and December 31st 2008. CAMELS-UK used the period from January 1st 1980 to December 31st 2012. LamaH used the period from January 1st 1989 to December 31st 2009. Finally, the observed historical E-OBS data covered the period between January 1st 1980 to December 31st 2018.

Mean annual values
The first climatic descriptors are the mean annual values for precipitation ($\overline{P}$), potential evaporation ($\overline{E_P}$), and temperature ($\overline{T}$). Theoretically, With more precipitation entering the soil the root-systems require less water to survive, resulting in low S_r values. It should be noted that this also depends on the seasonality of the precipitation as well as on the evaporation. Higher temperatures result in more potential evaporation which may increase the root-zone storage capacity.

Aridity Index
Based on these mean annual values the Aridity Index (AI) can be calculated. AI is the ratio of annual potential evaporation over annual precipitation (Equation 4.5). The parameter is a measure of the dryness of the climate at a given location. A low AI value means that the potential evaporation is relatively large compared to the precipitation, indicating arid circumstances. While a high AI value means that the amount of precipitation is large relative to the potential evaporation, indicating humid circumstances. Gao et al. (2014) suggests a positive correlation between the Aridity Index and the root-zone storage capacity.

$$AI = \frac{\overline{E_p}}{\overline{P}} \tag{4.5}$$

Holdridge Aridity Index
The Holdridge Aridity Index (HAI) is a variation of the Aridity Index, describing the climatic water availability of a catchment. HAI is defined as the ratio of the mean annual bio-temperature to the mean annual precipitation, making it an index of the potential evaporation rate (Shen et al., 2011). The mean annual bio-temperature is the value of the mean monthly temperature above freezing and below 30 °C. All values below freezing are adjusted to 0 °C, as plants are dormant at negative temperatures. Temperatures above 30 °C are adjusted to 30 °C as temperatures above 30 °C start to damage or kill the plants. HAI can be calculated using Equation 4.6.

$$HAI = \frac{58.93 \times \sum_{m=1}^{m=12} \overline{T_m}}{\overline{P}} \tag{4.6}$$

$\overline{T_m}$ is the monthly mean temperature in °C.

Seasonality Index
The Seasonality Index (SI), describes the yearly spread of precipitation. Equation 4.7 has been used to calculate this index. SI can fluctuate between 0 and $\frac{11}{6}$. If SI equals zero all months have equal amounts of precipitation, while a value of $\frac{11}{6}$ indicates that all precipitation occurs in one month (Guhathakurta & Saji, 2013). Gao et al. (2014) states that the root-zone storage capacity increases with an increase in the SI.

$$SI = \frac{1}{\overline{P}} \sum_{m=1}^{m=12} |\overline{P_m} - \frac{\overline{P}}{12}| \tag{4.7}$$

$\overline{P_m}$ is the mean monthly precipitation in mm.

Additional precipitation descriptors
For each catchment the following six descriptors have been determined. These descriptors contain information about the occurrence of high and low precipitation amounts. The low precipitation frequency (lpf) indicates the amount of dry days (< 1mm precipitation) that annually occur. Low precipitation duration (lpd) or interstorm duration (is_dur) indicates the maximum annual amount of consecutive dry days. Low precipitation timing (lpt) indicates in which season the most dry days occur. The high precipitation frequency (hpf) indicates the days during which the precipitation exceeds five times the annual mean daily precipitation amount. Using these days the high precipitation duration (hpd) and high precipitation timing (hpt) have been calculated using the same approach as for the dry days.

Seasonal variability indexes
Berghuijs et al. (2014) states that the seasonal variability of precipitation, potential evaporation, and temperature can be modelled as simple sinusoidal curves, using Equations 4.8, 4.9, and 4.10.

$$P(t) = \overline{P}[1 + \delta_P \sin(2\pi(t - s_P)/\tau_P)] \tag{4.8}$$

$$E(t) = \overline{E}[1 + \delta_E \sin(2\pi(t - s_E)/\tau_E)] \tag{4.9}$$

$$T(t) = \overline{T} + \Delta_T[\sin(2\pi(t - s_T)/\tau_T)] \tag{4.10}$$

t is the time in days, s stands for the phase shifts and τ indicates the duration of the seasonal cycle, which has been set to 1 year or 365 days. δ and Δ are dimensionless seasonal amplitudes, and the subscripts P, E, and T represent precipitation, potential evaporation, and temperature, respectively.

P(t), E(t), and T(t) represent the rates of precipitation [mm/d], potential evaporation [mm/d], and temperature [°C] as a function of time. The time-averaged mean values of these rates are given by $\overline{P}$, $\overline{E}$, and $\overline{T}$. The dimensionless seasonal amplitudes (δ_P, δ_E, and Δ_T) as well as the phase shifts (s_P, s_E, and s_T) have been determined using least squares optimization. The dimensionless seasonal amplitudes and the phase shifts are used in the regression analysis.

The phase difference between the precipitation and the temperature regime (s_d) can be computed using Equation 4.11 (Berghuijs & Woods, 2016). If sd = 0, the precipitation and temperature are completely in phase, sd = -0.5 indicates that the precipitation peaks before the temperature and sd = 0.5 indicates the precipitation to peak after the temperature.

$$s_d = s_P - s_T \quad \text{for} \quad |s_P - s_T| \leq 0.5 \tag{4.11a}$$
$$s_d = -1 + (s_P - s_T) \quad \text{for} \quad s_P - s_T > 0.5 \tag{4.11b}$$
$$s_d = 1 + (s_P - s_T) \quad \text{for} \quad s_P - s_T < -0.5 \tag{4.11c}$$

Seasonality Timing Index
Based on the parameters that have been calibrated by using the least square error optimization, the Seasonality Timing Index (ST) can be calculated. ST describes the seasonality of precipitation and whether the precipitation is in phase with the potential evaporation and temperature regimes.

$$ST = \delta_P sgn(\Delta_T) \cos(2\pi(s_P - s_T)/\tau) \tag{4.12}$$

Higher temperatures result in higher potential evaporation, therefore the equation only uses s_T. The ST value can range from -1 to 1. ST = 0 indicates uniform precipitation throughout the year. ST < 0 indicates that the signal is out of phase, with the precipitation being strongly winter dominant and ST>0 indicate that the precipitation is strongly summer-dominant. (Berghuijs et al., 2014)

Landscape descriptors

Besides climatic descriptors there are also several landscape descriptors that have been used for the regression. The catchment attributes that have been provided by the large sample data sets is the limiting factor when it comes to selecting these descriptors. In total seven descriptors have been classified, which can be divided into three categories, topography, land-use, and soil characteristics.

Topography
Two descriptors are used to describe the topography of a catchment, namely the mean elevation of a catchment and the mean slope.

Land-use
This category contains the forest fraction of the catchments. This fraction does not make any division between different types forests, but combines them all. Forests use a lot of water for transpiration, to survive dry periods they need a relatively large root-zone storage capacity.

Soil characteristics
This includes the soil porosity (soil_poros) and the fractions of sand, silt, and clay present in the soil (sand_frac, silt_frac, and clay_frac). It is expected that the composition of the soil has an impact on the root system of vegetation. de Boer-Euser et al. (2016) compared soil-derived and climate-derived root-zone storage capacities.

The climate data showed a higher explanatory power for the root-zone storage capacity, compared to the soil data. However, the combination of both climate and soil data was not investigated and might result in better values for the root-zone storage capacity.

Table 4.1: Overview of all catchment descriptors and their abbreviations.

Abbreviation	Catchment descriptor
$\overline{P}$	Mean Annual Precipitation
$\overline{T}$	Mean Annual Temperature
$\overline{Ep}$	Mean Annual Potential Evaporation
AI	Aridity Index
HAI	Holdridge Aridity Index
SI	Seasonality Index
hpf	High precipitation frequency
hpd	High precipitation duration
hpt	High precipitation timing
lpf	Low precipitation frequency
lpd	Low precipitation duration
is_{dur}	Interstorm duration
lpt	Low precipitation timing
δ_P	Seasonal precipitation amplitude
s_P	Phase shift of precipitation from reference date
Δ_T	Seasonal temperature amplitude
s_T	Phase shift of temperature from reference date
s_d	Phase difference between precipitation and temperature
δ_E	Seasonal potential evaporation amplitude
s_E	Phase shift of potential evaporation from reference date
ST	Seasonality Timing Index
mean_elev	Mean elevation
mean_slope	Mean slope
forest_frac	Forest fraction
soil_poros	Soil porosity
sand_frac	Sand fraction
silt_frac	Silt fraction
clay_frac	Clay fraction

4.2.3 Principal Component Analysis and K-means clustering

It can be difficult to identify pattern within large data sets. In this study, Principal Component Analysis (PCA) and K-means clustering are used to specify the relationship between the catchment descriptors and the root-zone storage capacity.

Principal Component Analysis

Principal Component Analysis (PCA) is a mathematical algorithm, that identifies patterns within the data by highlighting differences and similarities. The aim of this algorithm is to reveal the dominating characteristics of the given multivariate data set (Wold et al., 1987). Since managing large data sets can be quite challenging, the algorithm also aims to reduce the dimensions of the data set in order to increase the readability, without losing much of the information (Smith, 2002). PCA requires a matrix with N objects and K variables per object. The matrix should satisfy the following assumptions; the variables should be measured at a continuous level and linearly related, the matrix should be suitable for reduction and not contain any outliers, and the sample size must be adequate (> 150 objects).

PCA works with principal components to represent as much data as possible. Principal components of the data are variables constructed as linear combinations or

mixtures of the initial variables. These combinations are made so that the principal components are uncorrelated and contain as much information as possible in the first component. In other words, the first principal component (PC1) tries to explain as much data variance as possible. The second principal component (PC2) tries to explain as much as possible of the remaining variance. This process continues until there are an equal amount of principal components as there are variables in the matrix. The PCs are computed using the following steps. The first step is to standardize the data. This results in a data set for which each variable has a mean of zero. Based on this data the eigenvalues and eigenvectors are computed from the covariance matrix. The eigenvectors represent the directions of the axes where there is the most variance. These eigenvectors are the principal components. The eigenvalues are the coefficients that are attached to the eigenvectors, which contain information regarding the amount of variance that is explained. The eigenvector with the highest eigenvalue, explains the most variance and is therefore called PC1. PC2 should be uncorrelated to PC1, therefore this vector should be orthogonal to PC1. The eigenvector with the highest eigenvalue that is orthogonal to PC1 is called PC2. This process is continued until all principal components have been identified (Smith, 2002).

The results of a PCA are often visualized in a plot. The PCA-plot utilizes PC1 and PC2 as the axes of the figure. This approach makes it possible to plot the original data set using the linear combinations of all dimensions as described by the principal components. The amount of variance that is explained by each of the principal components is often given in the axis description of the plot. The amount of explained variance indicates the amount of initial data that is presented in the plot. In most cases the first two components are unable to explain 100% of the variance, meaning that part the information from the initial data set has been lost. However, based on the variance that is explained by the components, the main features of the data are still visible in the PCA-plots. The plots contain PC scores and loadings. The PC scores are all the dots that are present, which represent the objects of the matrix. This way, objects that plot close to each other show largely similar behavior for most of the variables that are considered. The loadings are visualized with vectors, which have a magnitude and a direction. Each vector represents a variable. The magnitude of the vector indicates the influence that the variable has on the principal component. The larger the vector, the higher the influence. The direction of the vectors can give information about the variables as well as the PC scores. If the vector is pointing in the direction of a group of PC scores, this indicates that this variable has a large positive influence on these scores. At the same time if the vector points in opposite direction, this variable is negatively correlated to these objects. If a vector is orthogonal to a group of scores, the variable is most likely not strongly correlated. The same principal applies to the vectors themselves. Vectors pointing in the same direction are positively correlated, when they point in opposite directions they are negatively correlated, and orthogonal vectors are not strongly correlated.

In this study the PCA has been utilized to determine the relationships between the root-zone storage capacity and the catchment descriptors as described in Section 4.2.2. The PCA objects are the selected catchments, while the variables are the catchment descriptors. From the PCA-plot it can be determined how the different catchment descriptors are related to the root-zone storage capacity.

K-means Clustering

The PCA-plot gives an overview of the objects with similar behavior and how they are related to the parameters. Therefore, this makes it possible to identify data clusters of similar functioning. To obtain these clusters a second assessment technique is used, called K-means clustering (MacQueen et al., 1967). K-means clustering is an iterative process that results in a user-specified number of clusters. The method starts by identifying a random point (centroid) for each cluster that should be cre-

ated. Each of the data points in the plot are then assigned to one of these centroids, after which the centroids move to the average of all its assigned data points. This process is repeated until the centroids no longer move as a result of the iterations, meaning that every point is assigned to the nearest centroid. This results in a number of clusters within which the objects show similar behavior.

In this study this technique can determine which catchment descriptors are important for the clustering of the data, providing information about the ability of a catchment descriptor to characterize a catchment. Additionally, comparing the root-zone storage capacity within each cluster can provide more insight to the influence of certain catchment descriptors on the root-zone storage capacity.

4.2.4 Multi-Linear Regression

The aim of this study is to propose a method with which the time-dynamic root-zone storage capacity can be estimated for the Meuse catchments. This means that the method can be applied to estimate the root-zone storage capacity for both the simulated historical and the simulated 2K climate data. Combining the past and future root-zone storage capacity results in a time-dynamic root-zone storage capacity. The proposed method is a regression relationship that is derived with Multi-Linear Regression (MLR). MLR is a technique that uses several independent variables to predict the outcome of a dependent variable. The mathematical formulation for this technique is given in Equation 4.13 (Schneider et al., 2010; Uyanık & Güler, 2013).

$$y = \beta_0 + \beta_1 x_1 + ... + \beta_n x_n + \epsilon \tag{4.13}$$

y = dependent variable
x_i = independent variables
β_0 = y-intercept (constant term)
β_i = regression coefficients for each of the independent variables
ϵ = error

The following assumptions are made when performing a MLR. It is assumed that there is a linear relationship between the dependent and independent variables. The data has been observed independently and has no significant outliers. There is no strong correlation between the independent variables, also called multi-collinearity. The data shows homoscedasticity, meaning the variance along the line of the best fit remains similar when moving up and down on the line and the errors of the regression line are normally distributed. In other words, the assumptions of MLR are linearity, independence, multi-collinearity, homoscedasticity, and normality. (Alexopoulos, 2010; Uyanık & Güler, 2013)

The performance of the MLR can be expressed in several ways. The most common method is the coefficient of determination (R^2). This statistical metric measures the amount of variation in the outcome that can be explained by the variation in the independent variables. Calculated using Equation 4.14, the value of R^2 can range from 0 to 1. If R^2 = 0 there is no relationship between the dependent and independent variable, if R^2 = 1 there is a perfect linear relationship between the variables (Schneider et al., 2010). The value of R^2 always increases when adding an independent variable to the regression. To eliminate this problem the adjusted R^2, also called the Ezekiel estimator, can be used. This number penalizes the R^2 formula based on the number of independent variables that the regression uses (Equation 4.15) (Chen & Liu, 2015). The adjusted R^2 value is lower compared to R^2 when it contains independent variables that do not impact the dependent variable.

Other methods to quantify the performance of the regression used in this study are: the Mean Error (ME), the Mean Absolute Error (MAE), and the Mean Absolute Per-

centage Error (MAPE). The formulas for these methods are given in Equations 4.16, 4.17, and 4.18, respectively.

$$R^2 = \frac{\sum_n^{i=1}(\hat{y}_i - \overline{y})^2}{\sum_n^{i=1}(y_i - \overline{y})^2} = \frac{\text{explained variance}}{\text{overall variance}} \tag{4.14}$$

$$\text{Adjusted } R^2 = 1 - \frac{n-1}{n-p-1}(1-R^2) \tag{4.15}$$

$$\text{Mean error (ME)} = \frac{1}{\text{n}} \sum_n^{i=1} (\hat{y}_i - y_i) \tag{4.16}$$

$$\text{Mean absolute error (MAE)} = \frac{1}{\text{n}} \sum_n^{i=1} \left|\hat{y}_i - y_i\right| \tag{4.17}$$

$$\text{Mean percentage error (MAPE)} = \frac{100}{\text{n}} \sum_n^{i=1} \left|\frac{y_i - \hat{y}_i}{y_i}\right| \tag{4.18}$$

n = Number of observations in the regression
$\hat{y}_i$ = The regression results for the dependent variable
y_i = The observed values for the dependent variable
$\overline{y}$ = The mean of the observed values for the dependent variables
p = Number of independent variables in the regression.

To get an estimate of the number of independent variables that are needed for the regression, the adjusted R^2 values have been plotted against the number of catchment descriptors. This gives an idea of the optimal amount of variables for the MLR. The amount of variables should be carefully considered, since the use of too little variables gives inaccurate results. On the other hand the use of too many variables increases the possibility of equifinality. Equifinality, is the notion that the chosen variables compensate for a wrong value. When applying the regression results to new data, this can result in large deviations (Fitzgerald, 2019).

Additionally, the regression must adhere to the assumption of no multi-collinearity. Therefore, all independent variables that are strongly correlated should not be considered in the same regression. These variable pairs are based on literature and have been verified with the results that are obtained from the PCA and K-means clustering. By eliminating these variable pairs, the possible combination of independent variables have decreased. The remaining combinations are investigated using multilinear cross-validation. In this study the Hold-out cross-validation method has been used. This method splits the available data into two non-overlapping parts. The first part is used for training (70% - 90%) and the second part was is for testing (10% - 30%) (Berrar, 2019). The MLR has been calibrated based on the training set, after which the resulting regression relationship was validated using the test set. This reduces the possibility of equifinality resulting in a more accurate estimation for the generalized performance of the regression (Refaeilzadeh et al., 2009). This process has been repeated multiple times. For each iteration the best regression relationships have been selected based on the adjusted R^2 values of the test set. These relationships have then been further investigated by comparing the performance for the Meuse catchments, using the ME, MAE, and MAPE values.

In this study the MLR is executed using the Ordinary Least Squares method. The dependent variable is the root-zone storage capacity, and the independent variables is formed by the catchment descriptors. To determine the performance of the regression, the MLR is comparing the outcomes to the S_r values that result from the water balance method. Based on the MLR results and the ability of the regression

to predict the root-zone storage capacity for the Meuse catchments, a relationship is selected. This regression relationship is used to estimate the time-dynamic root-zone storage capacity for the Meuse catchments.

4.3 The Wflow_FLEX-Topo model to evaluate the impact of a time-dynamic root-zone storage capacity

The Wflow_FLEX-Topo model has been used to evaluate the impact of a time-dynamic root-zone storage capacity on the change in the hydrological response of the Meuse catchments as a result of 2K climate change. In this section the model is explained, followed by an explanation regarding the application of this model within this study.

4.3.1 The Wflow_FLEX-Topo model

The Wflow_FLEX-Topo model is a fully-distributed process-based model. The model uses a Flux Exchange (FLEX) modelling approach, meaning that the relevant hydrological processes within the catchments have been represented by a combination of reservoirs and transfer functions (Fenicia et al., 2006). The spatial variability of the hydrological processes within a catchment have been simulated by different configurations of reservoir and transfer functions. These different configurations are also called Hydrological Response Units, HRUs. The Wflow_FLEX-Topo model has specified three different HRUs, called wetlands, hillslopes, and plateaus. Table 4.2 contains the thresholds that are used to determine which HRU should be used to model an area within a catchment (Gharari et al., 2011).

The model input consists of distributed precipitation, temperature, and potential evaporation data. The different HRUs are all connected to each other through the common groundwater storage S_s [mm]. Moreover, all HRUs include storage for snow S_W, interception S_I, root-zone S_R, and a fast runoff component S_F, as well as transfer functions for Evaporation [mm d^{-1}] from snow storage (E_W), interception storage (E_I), and the root-zone storage (E_R). The total streamflow Q [mm d^{-1}] is made up of the groundwater runoff Q_s and the fast runoff Q_F from the different HRUs (Bouaziz et al., 2021). Figure 4.4 gives a schematic overview of these storage and transfer functions within the model.

The main differences between the HRUs include potential differences in parameter values. In Figure 4.4, the subscripts P, H, and W are used to distinguish between the Plateaus, Hillslopes, and Wetlands respectively. Other differences are the presence of percolation in the plateau class, while this is not present in the other HRUs. Moreover, the wetlands include capillary rise but exclude preferential recharge (Bouaziz et al., 2021). Appendix C provides a definition for the different fluxes and storage of Figure 4.4. An overview of the water balances and the equations for each of the HRUs can be found in the supplements of Bouaziz et al. (2021).

Bouaziz et al. (2021) has calibrated the model for the Meuse catchments. The calibration was done using the streamflow at Borgharen and the observed historical E-OBS meteorological data. The calibration used the data from 2007-2011, with 2005-2006 as warm-up years, and the period from 2012-2017 as the post-calibration period. This data has been used as it is assumed to most closely represent the current-day conditions. The aim of the calibration was to retain an ensemble of plausible realizations, to optimally reflect different aspects of the hydrograph. The seasonal streamflow regime is relatively well reproduced by the model, as the four objective functions show a relatively similar performance during calibration and evaluation, with median values of approximately 0.93 and 0.78 for Borgharen and for the 35 catchments of the Meuse, respectively (Bouaziz et al., 2021).

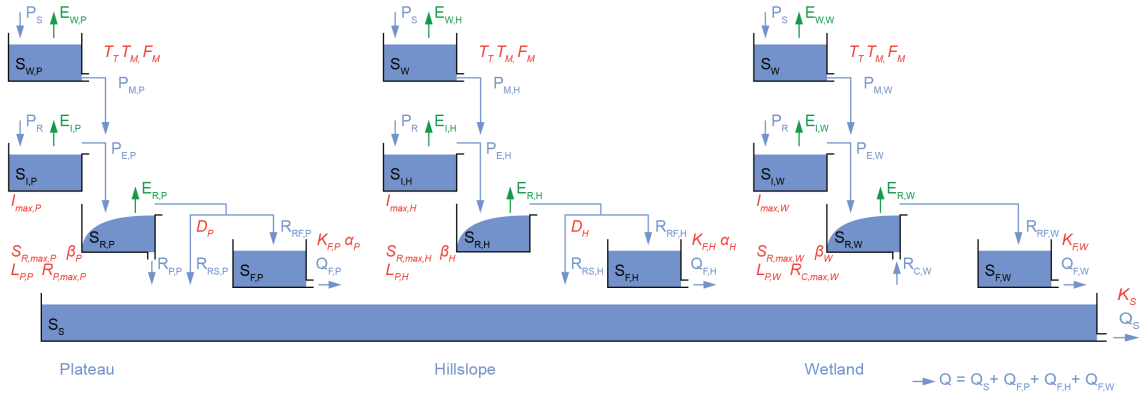

Figure 4.4: Schematic overview of the Wflow_FLEX-Topo model structure. The subscripts P, H, and W are used for the Plateaus, Hillslopes, and Wetlands respectively (source: (Bouaziz et al., 2021)).

Table 4.2: The threshold values for the different Hydrological Response Units (HRUs).

	Wetlands	Hillslope	Plateau
Height Above the Nearest Drainage (HAND) [m]	<5.9	N/A	>5.9
Slope [-]	<0.125	>0.125	<0.125

4.3.2 Evaluating the change in hydrological response

Figure 4.5, gives an overview of the way in which the Wflow_FLEX-Topo model has been used in this study. The model has been used to evaluate the impact that a time-dynamic root-zone storage capacity has on the change in hydrological response. This impact is quantified with the use of 3 different model scenarios. Each scenario consists of a part that models the historical hydrological response, which is forced using the simulated historical climate data, and a part that represents the future hydrological response which is forced using the simulated 2K climate data. The impact that the time-dynamic root-zone storage capacity has on the change in hydrological response is determined by subtracting the results of the historical part of the model from the results of the 2K part of the model. Besides the root-zone storage capacity, all other parameters have remained static for the model runs.

Scenario 1: Benchmark - Water balance method
In scenario 1 it is assumed that the vegetation has not adapted its root-zone storage capacity as a result of the 2K climate. The root-zone storage capacity has been computed using the simulated historical climate data and the water balance method that is explained in Section 4.1. These values have been used in both the historical and 2K run of the model. This scenario implies all model parameters to be static and can be seen as the benchmark scenario for the water balance method.

Scenario 2: Benchmark - Regression relationship
In scenario 2 the same assumption has been applied. However, this time the root-zone storage capacity has been estimated using the regression relationship that is explained in Section 4.2. This relationship has been applied to the simulated historical climate data of the Meuse to obtain root-zone storage capacity estimates for each of the 35 catchments. These values have been used in both the historical and 2K run of the model. This scenario implies all model parameters to be static and can be seen as the benchmark scenario for the regression relationship.

Scenario 3: Dynamic - Regression relationship
In Scenario 3 it is assumed that vegetation has adapted its root-zone storage capacity as a result of the globally 2K warming climate. The simulated historical climate data is used to estimate the root-zone storage capacity for the historical run and the sim-

ulated 2K climate data is used to estimate the root-zone storage capacity for the 2K run. It should be emphasized, that both root-zone storage capacities have been estimated with the regression relationship. This scenario no longer implies a stationary root-zone storage capacity and is therefore called the dynamic regression scenario.

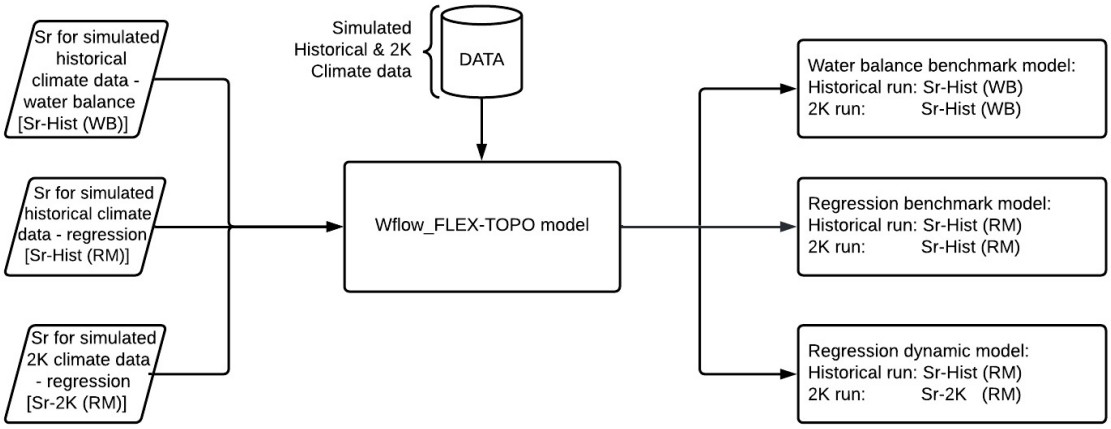

Figure 4.5: Flow diagram for the use of the Wflow_FLEX-Topo model in this study.

Evaluation
Each scenario that is discussed gives an indication of the change in hydrological response when comparing the 2K climate run with the historical climate run. This response is quantified by plotting the change in mean monthly hydrological response of several flux and state variables between the 2K and historical model run, namely the streamflow (Q), actual evaporation (E_A), root-zone storage (S_r), and groundwater storage (S_s).

The only changing component within the benchmark scenarios is the forcing data that is used for the 2K run. The results of these scenarios therefore give the change in hydrological response that results from this difference in forcing data. When comparing the benchmark scenarios with each other, the only difference is the method with which the root-zone storage capacities are estimated. Therefore, by comparing the benchmark for the regression relationship with the benchmark for the water balance method, we can quantify the impact that the regression method has on the change in mean monthly hydrological response.

For the dynamic regression model scenario, the forcing data and the root-zone storage capacity were changed for the 2K run of the model. In other words, it used a time-dynamic root-zone storage capacity in comparison to the static root-zone storage capacity that has been used in the benchmark scenarios. Both the regression benchmark scenario and the dynamic regression scenario have used the regression relationship to obtain the root-zone storage capacities. Therefore, the only difference between these model scenarios is the static versus the time-dynamic root-zone storage capacity. By comparing the dynamic regression to the regression benchmark scenario, we can quantify the impact that the time-dynamic root-zone storage capacity has on the change in mean monthly hydrological response.

5 | Results

This section presents the results of the root-zone storage capacity computations using the water balance method (Section 5.1), followed by the results of the regression relationship (Section 5.2). In Section 5.3 the differences between the results from these two methods are discussed for the simulated climate data sets of the Meuse catchments. Lastly, the Wflow_FLEX-Topo model is used to evaluate the difference in hydrological response of the Meuse basin, when using a static root-zone storage capacity compared to a time-dynamic root-zone storage capacity (Section 5.4).

5.1 Root-zone storage capacity estimates based on the water balance method

The root-zone storage capacities are estimated using the water balance method, as explained in Section 4.1. The root-zone storage capacities for the simulated historical climate data of the Meuse (Sr-Hist$_{\mathrm{WB}}$) range between 140 and 291 mm as shown in Figure 5.1b. The exact magnitudes of these root-zone storage capacities have been provided in Appendix D. The Sr-Hist$_{\mathrm{WB}}$ values are used as reference values to determine how well the regression method can predict the root-zone storage capacity of the Meuse catchments. Additionally, they are also used in the Wflow_FLEX-Topo model, as part of the water balance benchmark scenario (Section 5.4).

Part of the data processing consisted of plotting the catchments in the Budyko framework. The Aridity Index is estimated by relating the long-term average potential evaporation to the long-term average precipitation. The Evaporative Index relates the long-term actual evaporation to the long-term precipitation. The actual evaporation is estimated by subtracting the streamflow out of the system from the incoming precipitation. Figure 5.1a indicates the position of the different Meuse catchments and shows that two catchments exceed the energy limit that is provided by the Budyko framework. The two catchments that plot on the left side of the energy limit are Beverce and La Sormonne. This indicates that in these catchments the estimated actual evaporation exceeds the estimated potential evaporation. These differences could be the result of deep underground discharge or water subtraction by human activities. Since the data does not provide enough information to account for these differences, the root-zone storage capacities would not provide accurate results. These catchments have been given the same root-zone storage capacities as one of their neighbouring catchments, as the Wflow_FLEX-Topo model requires a S_r value for all catchments. Beverce catchment received the same root-zone storage capacity as Maastricht catchment and La Sormonne Belval received the same root-zone storage capacity as La Bar Cheveuges catchment (Figure 5.1b). These neighbouring catchments have been chosen based on the similarity in hydrological data.

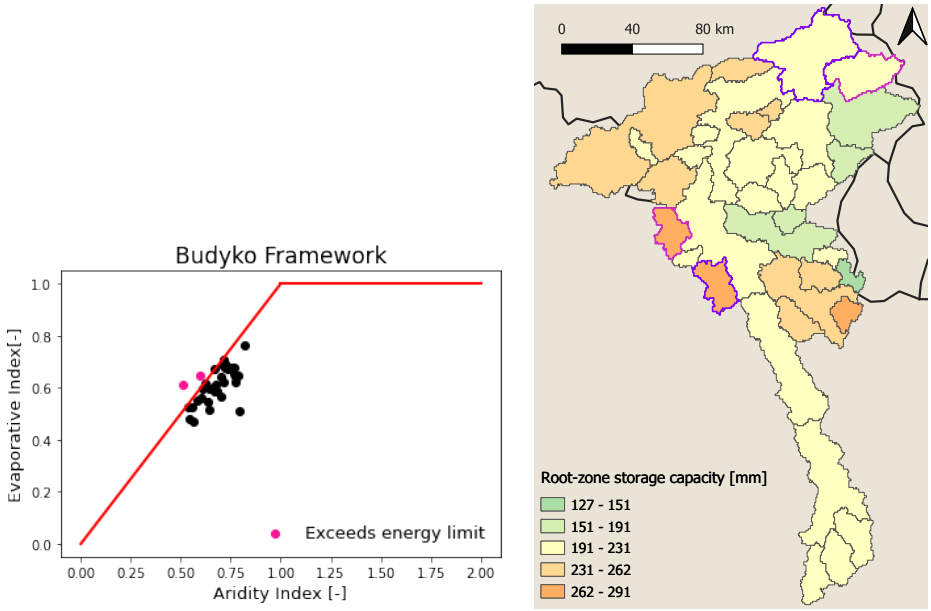

Figure 5.1: (a) The Budyko framework of the Meuse catchments from the simulated historical climate data. (b) The Meuse catchments, and the root-zone storage capacity estimates for the simulated historical climate data using the water balance method (Sr-Hist$_{WB}$). Catchments exceeding the energy limit have a pink border (Beverce and Sormonne Belval). The purple border indicate the catchments which root-zone storage capacity has been used for the pink catchments (Maastricht and La Bar Cheveuges).

5.2 Deriving the regression relationship

This section describes the results of the regression relationship used to estimate the root-zone storage capacity for the simulated historical and 2K climate data. First, the catchment selection is discussed (Section 5.2.1), followed by the root-zone storage capacities computed with the water balance method (Section 5.2.2), and the catchment descriptors that are used as the input for the MLR analysis (Section 5.2.3). The results of the PCA and K-means clustering that have been performed with this data are described in Section 5.2.4. This is followed by the Multi-Linear Regression analysis, which resulted in the regression relationship that is used to estimate the root-zone storage capacities of the Meuse catchments for historical and future conditions (Section 5.2.5).

5.2.1 Catchment selection

For the catchment selection each of the catchments has been screened in order to determine whether it is suitable for the analysis. The requirements state that the catchments should have minimal human impact and less than 10% of the annual precipitation can consist of snowfall. The amount of human impact has been determined based on the information provided by each of the data sets.

CAMELS-USA
The CAMELS-USA data set contains 671 catchments. All initial catchments are characterized by low human impact, meaning no catchments have been eliminated due to this requirement (Newman et al., 2015). This in contrast to the snowfall requirement, which resulted in the elimination of 331 catchments. The data sets were selected in order to find catchments in similar climatic conditions as the current or future Meuse. Therefore, the choice was made to only consider catchments on the East Coast. This requirement resulted in an additional elimination of 135 catchments. The remaining catchments have been processed and checked for data availability, which resulted

in the elimination of 18 catchments. Finally, we kept a total of 187 catchments that were suitable for the analysis.

CAMELS-GB
The CAMELS-GB data set provides information on the human impact in each of the catchments. The human impact has been determined by data on reservoirs, abstraction, and discharge returns. For this study only the UK Benchmark Network catchments have been used. These catchments are characterised by modest influence of humans on the flow regimes and can be treated as relatively 'near-natural' (Coxon et al., 2020). Based on this 534 catchments could be eliminated, as they did not adhere to the requirement of minimal human influence. An additional 6 catchments have been eliminated due to the snowfall requirement. Finally, data processing and availability resulted in the additional elimination of 3 catchments. The remaining 128 catchments have been used in the analysis.

LamaH
From the 859 catchments present in the LamaH data set, 454 catchments were identified to have minimal human impact (Klingler et al., 2021). Since the catchments are located in a mountainous area, the snow impact is significant in the majority of the catchments, resulting in the elimination of 309 catchments. An additional 42 catchments have been eliminated, as the result of processing and missing streamflow data. Resulting in a total of 103 catchments that are suitable for the analysis.

Observed historical E-OBS data
The observed historical E-OBS data has been processed. Similar to the simulated historical climate data the Beverce and La Sormonne Belval catchments, exceeded the energy limit. As previously discussed, this could be caused by for example, deep underground discharge or water subtraction by human activities. Since the data shows a deviation, the decision was made to eliminate these two catchments from the analysis. The remaining catchments have all been used as part of the analysis.

From the approximately 2200 catchments that are present in the data sets, 451 catchments could be used in this study. Figure 5.2 gives an overview of the locations of these catchments.

5.2.2 Computing the root-zone storage capacities with the water balance method

The performance of the regression relationship is determined based on its ability to reproduce the root-zone storage capacity values as computed with the water balance method. The regression uses the selected catchments from the large sample data sets, as well as the catchments from the observed historical E-OBS data. The results of the S_r computations for these catchments have been visualized in Figure 5.2. The root-zone storage capacities range from 36 to 499 mm. Figure 5.2, clearly shows that there is a geo-spatial spread when it comes to S_r. The lowest values are found in the Northern part of Great-Britain, from where the values increase towards the Southeast. The highest values are found in the center of the United States, with decreasing values towards the East coast. The LamaH and observed historical E-OBS data contain average root-zone storage capacity values. This geo-spatial spread suggests that the value of S_r depends on the climatic conditions in a region. This suggestion is further validated by the position of the catchments within the Budyko framework as shown in Figure 5.3. The figure indicates that the current position of the Meuse catchment overlaps with catchments from each of the large sample data sets. Additionally, the root-zone storage capacity shows an increase with increasing values for the Aridity and Evaporative Index. Global warming will likely result in a shift of the Meuse catchments within the Budyko framework, towards increasing

values for the Aridity and Evaporative index. Therefore, the root-zone storage capacities of the Meuse catchments might increase in future climate conditions.

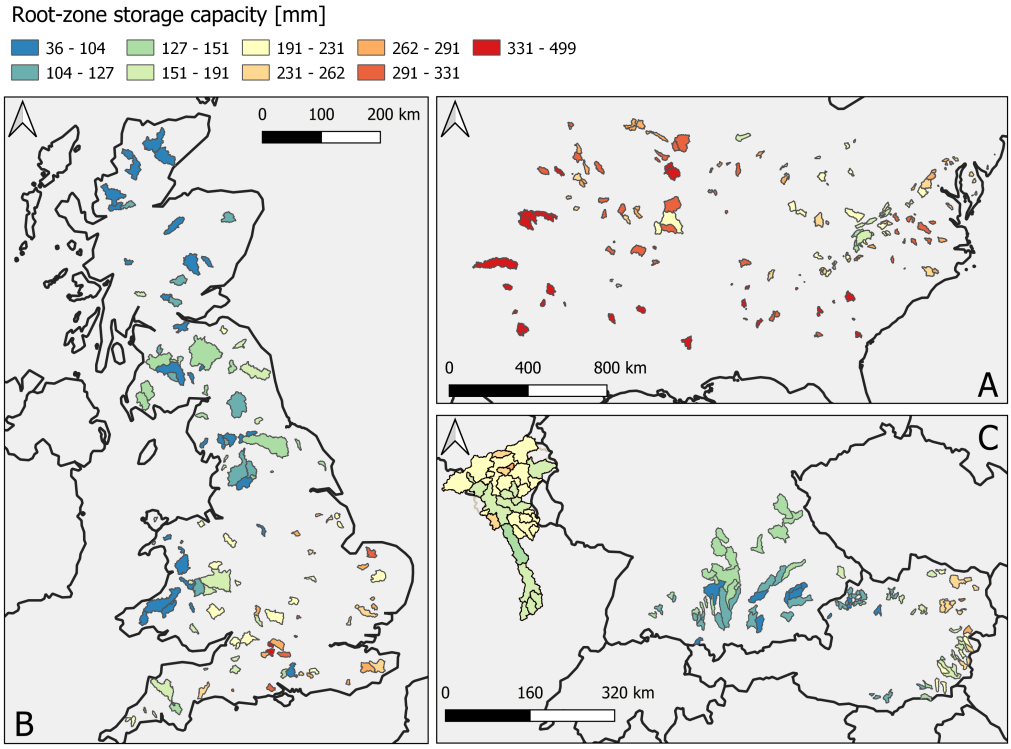

Figure 5.2: The selected catchments and their respective root-zone storage capacities computed with the water balance method (a) CAMELS-USA, (b) CAMELS-GB, (c) LamaH, and the observed historical E-OBS data

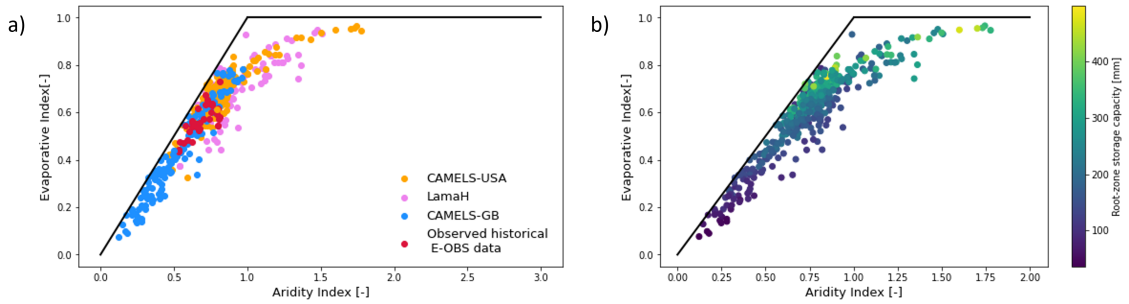

Figure 5.3: (a) The location of the selected catchments within the Budyko framework. (b) The variation of the root-zone storage capacity in the Budyko framework, the magnitude of the root-zone storage capacity is indicated by the colour scale.

5.2.3 Computing the catchment descriptors

The catchment descriptors have been computed for the selected catchments as explained in Section 4.2.2. The Python scripts that have been used for these computations are provided in Appendix B.

5.2.4 Principal Component Analysis and K-means clustering

PCA has been performed using the root-zone storage capacities and the catchment descriptors that have been described in the previous sections. The 451 catchments form an adequate sample size with which PCA can be performed.

The results of the PCA have been visualized in Figure 5.4. Figure 5.4a shows the loadings of the climatic descriptors, while Figure 5.4b shows the loadings of the landscape descriptors. These loadings have been separated into two plots for readability purposes. The axes of the figure indicate that PC1 and PC2 explain 38.2% and 16.1% of the range, respectively. In other words, the plot contains 54.3% of the information provided by the initial data.

The loading vectors that have been visualized in Figure 5.4 contain additional information regarding the inter-correlations of the input data. The input data consisting of the root-zone storage capacities and the catchment descriptors, which are all represented in the plots. The root-zone storage capacity has been added to both plots by the abbreviation 'Sr_20_yr'. The plots show that the root-zone storage capacity is positively correlated with: annual temperature and potential evaporation ($\overline{T}$, $\overline{E_P}$), Holdridge Aridity Index (HAI), high precipitation frequency and duration (hpf, hpd), low precipitation frequency and duration (lpf, lpd), and forest fraction (forest_frac). The root-zone storage capacity is clearly negatively correlated with: Seasonality Index (SI), phase difference between precipitation and temperature (s_d), seasonal potential evaporation and precipitation amplitude (δ_E, δ_P), Seasonality Timing index (ST), high precipitation timing (hpt), sand fraction, mean slope, and mean elevation. The remaining catchment descriptors that do not show a strong correlation to the root-zone storage capacity are annual precipitation ($\overline{P}$), Aridity Index (AI), phase shift of precipitation, temperature, and potential evaporation (s_P, s_T and s_E), seasonal temperature amplitude (Δ_T), low precipitation timing (lpt), soil porosity, and fraction of silt and clay (silt_frac, clay_frac).

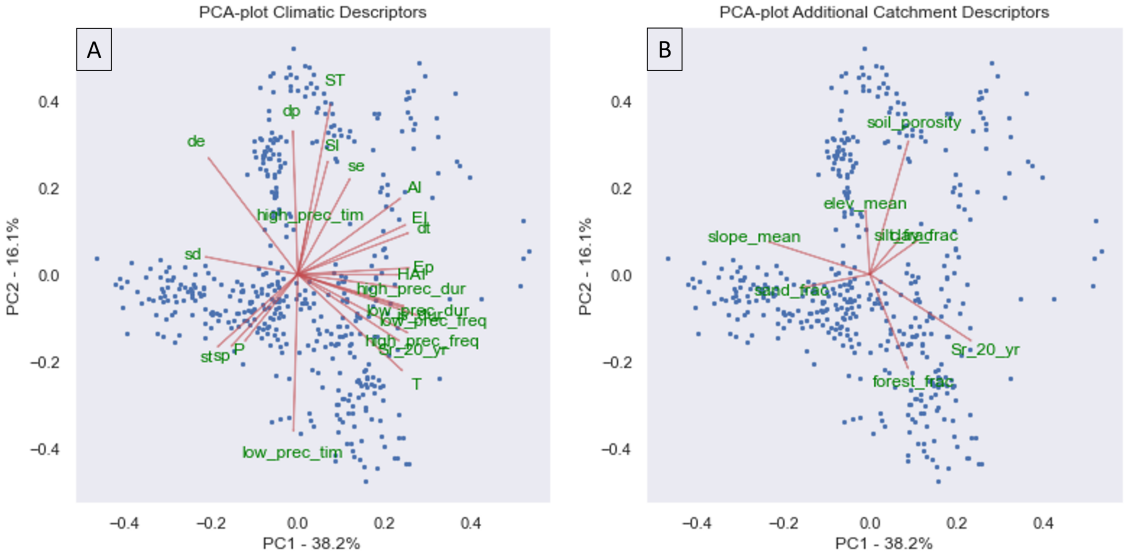

Figure 5.4: The PCA-plot for (a) climatic descriptors, (b) landscape catchment attributes. 'Sr_20_yr' indicates the loading for the root-zone storage capacity.

The K-means clustering approach is used to identify catchment clusters of similar functioning, since catchments that plot closely together in the PCA-plot have shared descriptor variables. In total 6 different clusters have been identified. Figure 5.5a shows the clusters within the PCA-plot and indicates the data set from which the catchment originates. The Meuse catchments are part of cluster 4 and has been visualized by a black border in the figures. The root-zone storage capacity in this cluster ranges between approximately 200 and 270 mm, as shown in Figure 5.5b. This

figure also shows that each of the clusters has their own range of root-zone storage capacities, which indicates that different catchment descriptor values result in different root-zone storage capacities. Boxplots for each of the catchment descriptors have been provided in Appendix E. Based on these boxplots the main characteristics of each cluster are determined. An overview of the geo-spatial spread of the clusters and their main characteristics is shown in Figure 5.6.

Cluster 2 contains the catchments with the lowest root-zone storage capacities. This cluster contains mainly catchments from the CAMELS-GB data set. The catchments are characterized by high annual precipitation and low values for both the high and low precipitation frequency. Moreover, these catchments are characterized by low annual potential evaporation and temperatures. Cluster 1 also contains catchments with low root-zone storage capacities. These catchments are mainly located in Central Europe and are characterized by the low values for temperature and high and low precipitation frequency. Additionally, they have a relatively high Seasonality Index, which explains the low root-zone storage capacity values.

The catchments of clusters 4 and 5 have average root-zone storage capacities. Cluster 4 consists of catchments from all the data sets that have been used in the clustering, while cluster 5 consists mainly of catchments from the CAMELS-USA data. The clusters are characterized by a low Seasonality Index, which indicates the presence of uniform precipitation throughout the year. Additionally, they contain average values for the low and high precipitation frequency. The clusters can be distinguished from each other, as cluster 4 is characterized by low annual temperature and potential evaporation values, while cluster 5 is characterized by high annual potential evaporation values.

Clusters 0 and 3 consist of CAMELS-USA catchments. These clusters have high root-zone storage capacity values and can be characterized by high annual potential evaporation and temperature values. Both clusters also show high values for the high and low precipitation frequencies. They can be distinguished from one another as cluster 3 is characterized by high SI and AI values and low annual precipitation values, while cluster 0 can be characterized by low Seasonality Timing Index and high annual precipitation value.

To conclude, the PCA in combination with the K-means clustering have clustered the catchments based on similar functioning. A clear distinction between the relevant catchment descriptor variables and the root-zone storage capacity in the different clusters can be made, which indicates that S_r is indeed described by different variable values in different regions. This forms the basis on which the Multi-Linear Regression has been performed.

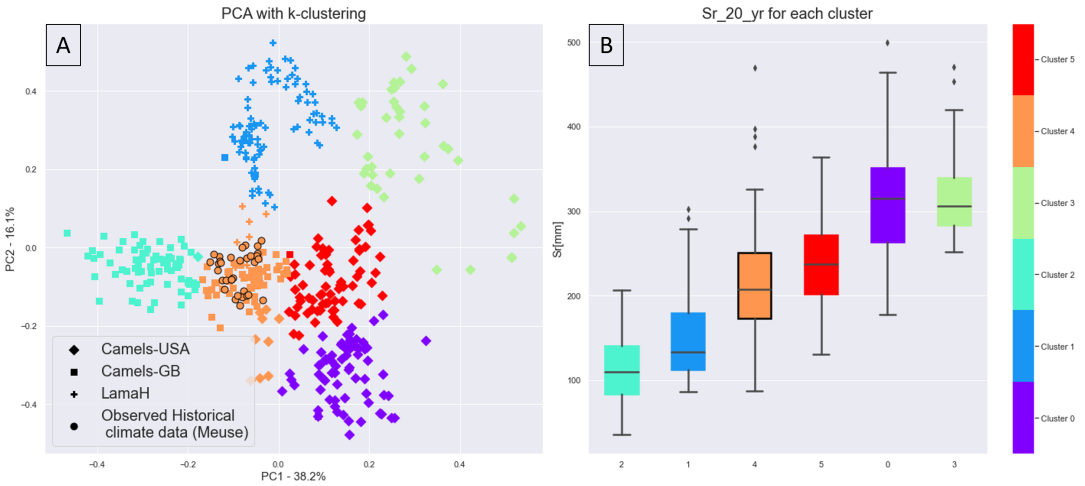

Figure 5.5: (a) PCA-plot indicating clusters with catchments of similar functioning as well as the origin of the catchments in the clusters. (b) Boxplot visualizing the range of the root-zone storage capacity within each cluster. In both figures the black border indicates the position of the observed historical E-OBS catchments.

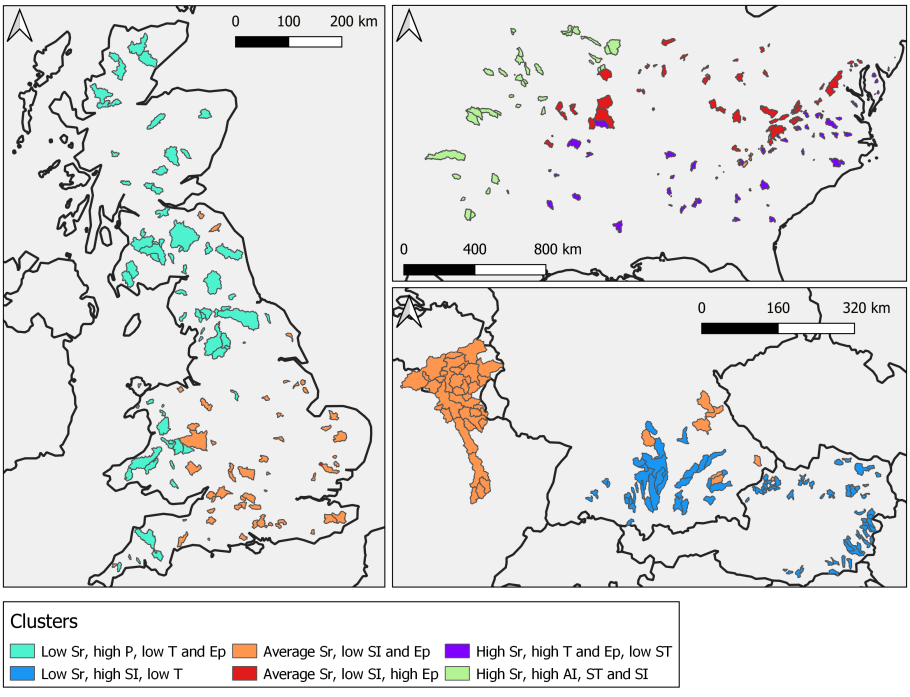

Figure 5.6: Geo-spatial distribution of functional catchment clusters.

5.2.5 Multi-Linear Regression

Multi-Linear Regression Analysis has been applied to the catchment descriptors, resulting in a relationship that can be used to estimate the root-zone storage capacity for the simulated historical and 2K climate data. The MLR has been developed with the use of the root-zone storage capacities computed with the water balance method.

To determine the optimal number of independent variables that should be used in the regression, the adjusted R^2 value has been plotted against the number of independent variables. Figure 5.7 indicates that the adjusted R^2 value increases up until the use of 6 independent variables, after which the curve flattens at a value of approximately 0.76. Since there are minimal increases in adjusted R^2 when using more than 6 independent variables, this study will focus on regression results that consider 6 or less independent variables.

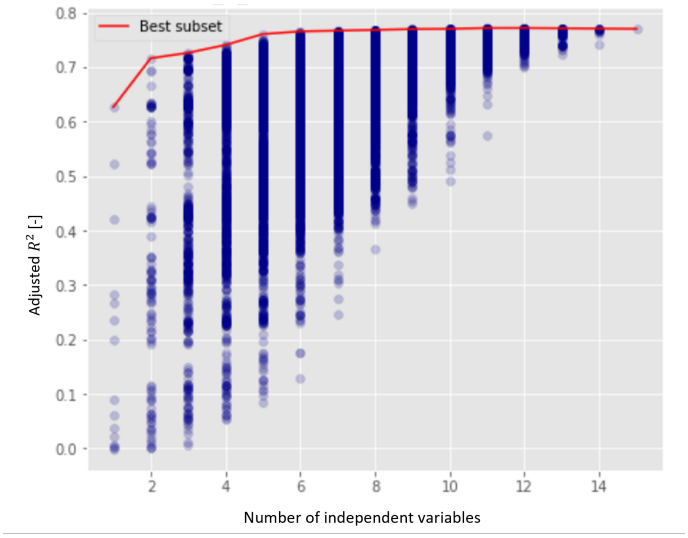

Figure 5.7: The adjusted R^2 value plotted against the number of independent variables in the regression

The regression model must adhere to the assumption of no multi-collinearity. However, this assumption is not valid for all the catchment descriptors. For example, the mean annual potential evaporation is used to compute the Aridity Index, which makes these variables strongly correlated. Any change in potential evaporation will directly change the Aridity Index. To make sure that the assumption of no multi-collinearity is met by the regression, strongly correlated descriptors are not allowed to be part of the same model. A complete list of strongly correlated descriptors is provided in Appendix F.

Cross-validation has been applied decreasing the possibility of equifinality, producing a more accurate regression. The total of 451 catchments that are considered in the MLR have been randomly divided into a training data set and a test data set. The training data set contains 380 catchments (∼84%), leaving 71 catchments (∼16%) for the test data set.

After eliminating the strongly correlated catchment descriptors and specifying the division of the data, the Multi-Linear Regression with cross-validation has been executed. The regression has been executed multiple times for each possible combination of catchment descriptors, using different test and training data sets. From these iterations we identified the regression relationships with the highest adjusted R^2 value for the test data. The independent variable combinations that created these values have been further investigated. This process has been executed for models containing 2 to 6 independent variables. For each iteration the five best performing regression relationships for each of these models is provided in Appendix G. For the

models containing 2 to 6 independent parameters, the best regressions resulted in adjusted R^2 values of 0.71, 0.74, 0.72, 0.75, and 0.73, respectively. This shows that the regression performance is not drastically impacted by the addition of an independent variable.

The regression relationships that are identified by the iterations have been further investigated with the use of the PCA results. From the PCA it has been determined whether there is a positive, negative or weak relationship between each of the catchment descriptors and the root-zone storage capacity. Based on this information the sign of the regression coefficients has been checked. A positive relationship between the catchment descriptor and the root-zone storage capacity should be represented by a positive regression coefficient. A negative relationship should be represented by a negative regression coefficient. The regression models that did not adhere to this principle have been eliminated from the selection.

After this additional validation, the best performing regression relationships have been selected for each of the models with 2 to 6 independent variables. This selection has been based on the ability of the regression to predict the root-zone storage capacity of the Meuse catchments for the observed historical E-OBS data and the simulated historical climate data. The performance of the 2 to 6 variable models have been quantified by the ME, MAE, and MAPE values of 1000 iterations with the different regression relationships. This process resulted in the selection of one regression relationship for each of the 2 to 6 variable models. Table 5.1 shows the regression relationships and the median of R^2 and adjusted R^2 for the training and test data. From this table it can be concluded that the differences in model performance are relatively small. The R^2 of the training and test data ranges between 0.70-0.73 and 0.67-0.72, respectively. The adjusted R^2 of the training and test data ranges between 0.70-0.73 and 0.67-0.70, respectively.

Figure 5.8 shows boxplots for the iterations of the models that are indicated in Table 5.1. The first graph shows the R^2 and adjusted R^2 values for both the training and test data of the different models. These boxplots show that the addition of a third independent variable has some effect on the performance of the model as it increases the R^2 and adjusted R^2 between 0.01 and 0.05. However, the addition of a fourth, fifth, or sixth independent variable changes the R^2 and adjusted R^2 with values between -0.02 and 0.02. The remaining graphs in Figure 5.8 show the ME, MAE, and MAPE boxplots for different parts of the data. The boxplots represent model values for training data, test data, observed historical E-OBS data, and simulated historical climate data for the Meuse catchments. The boxplots for the training and test data show that the ME values plot around the zero line, which is expected, since the aim of a multi-linear regression is to minimize the mean error. For the MAE the values of these categories show a decrease with increasing independent variables. The median for the training data decreases from 37.61 to 34.19 mm and the test data decreases from 38.11 to 34.33 mm. This means that the root-zone storage capacity computed with the regression model deviates on average around 35 mm compared to the value computed with the water balance method. The MAPE boxplot shows the same decrease for the training and test data, the decrease is approximately 20-18% and 20-19%, respectively.

The ME for the observed historical E-OBS data has a negative value for the model with 2 independent variables, and has positive values for the remaining models. The ME for the simulated historical climate data has negative values for all models. The 4 and 6 variable models result in the smallest ME values. The MAE shows the same pattern for the simulated historical climate data, with the smallest error in the 4 and 6 parameter models. The MAE for the observed historical E-OBS data shows a decrease with increasing independent variables, however this decrease is relatively small.

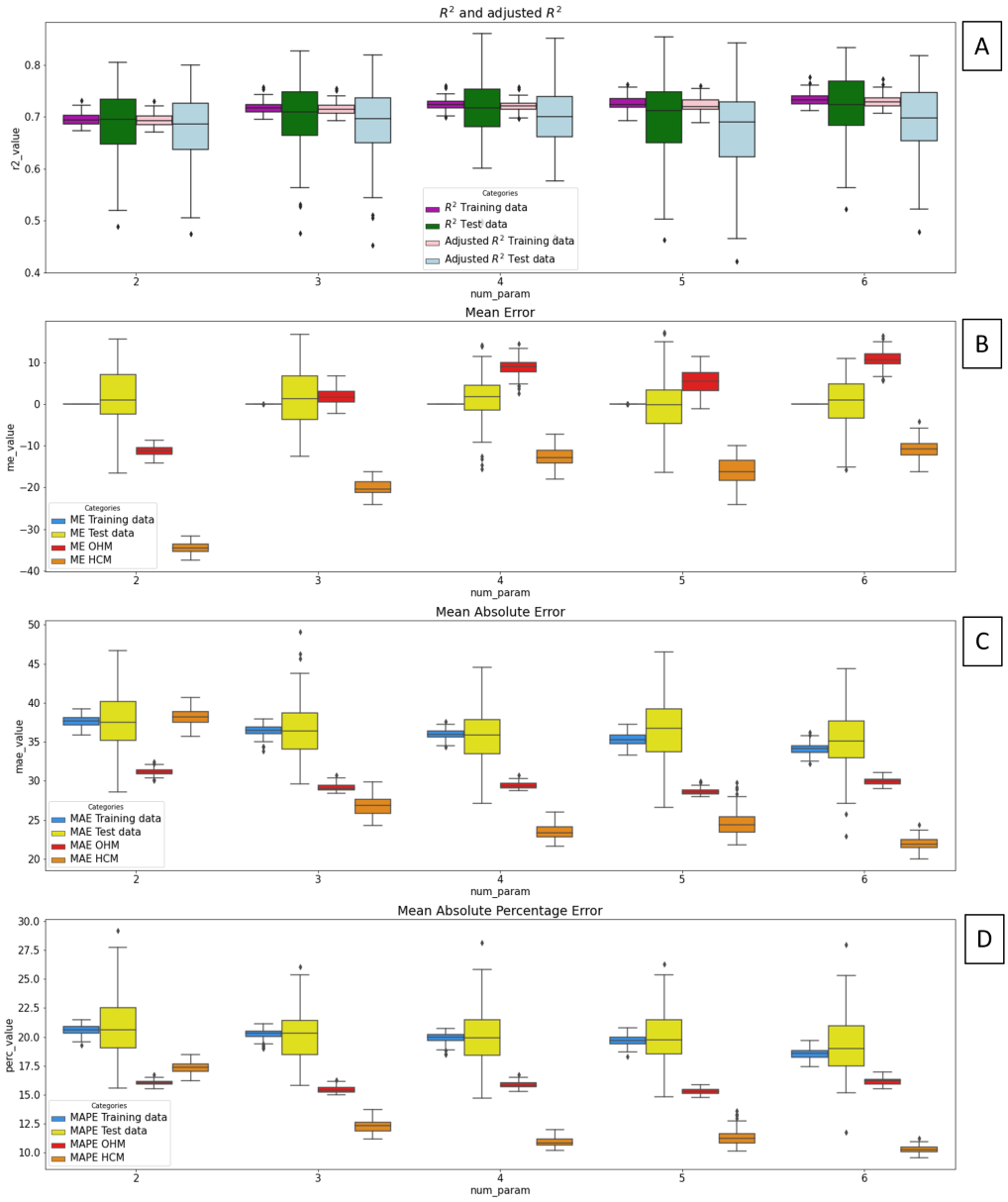

Figure 5.8: The performance of the different independent variable models, based on different parts of the data set (a) the R^2 and adjusted R^2 values for the training and test data. (b) The mean error (ME), (c) the mean absolute error (MAE), and (d) the mean absolute percentage error (MAPE). Boxplots b,c, and d show the values of the training and test data as well as for the simulated historical climate data (HCM) and the observed historical E-OBS data (OHM) of the Meuse catchments

Table 5.1: The R^2 and adjusted R^2 values for the training and test data of the selected regression relationships for each of the models with 2 to 6 independent variables.

Independent variables	R^2 **Training data**	R^2 **Test data**	**Adjusted** R^2 **Training data**	**Adjusted** R^2 **Test data**
HAI, δ_E	0.70	0.67	0.70	0.67
HAI, s_P, δ_E	0.72	0.71	0.71	0.70
HAI, s_P, δ_E, sand-frac	0.73	0.69	0.72	0.68
HAI, s_P, δ_E, silt-frac, SI	0.72	0.71	0.72	0.69
HAI, s_P, δ_E, sand-frac, E_P, forest-frac	0.73	0.72	0.73	0.70

The models are of similar performance, which makes it difficult to decide which model should be used. A balance must be found between the number of variables and the

performance of the model. When computing the root-zone storage capacity for the simulated historical climate data the model with 4 or 6 variables are the most promising. Since the model with 4 independent variables has less variables, this model is preferred over the model with 6 variables. The observed historical E-OBS data catchments are also relatively well predicted by the 4 variable model. Therefore, the model with 4 independent variables has been selected as the best performing model. The model has a Mean Absolute Percentage Error of 11% for the historical climate data of the Meuse and 15% for the observed historical E-OBS data. The independent variables that make up this model are Holdridge Aridity Index (HAI), phase shift of precipitation (s_P), seasonal amplitude for the potential evaporation (δ_E), and sand fraction (sand_frac). The equation that results from these variables is given in Equation 5.1.

$$S_r = \beta_0 + \beta_{HAI} * HAI + \beta_{sp} * sp + \beta_{de} * de + \beta_{sand_{frac}} * sand_{frac} \tag{5.1}$$

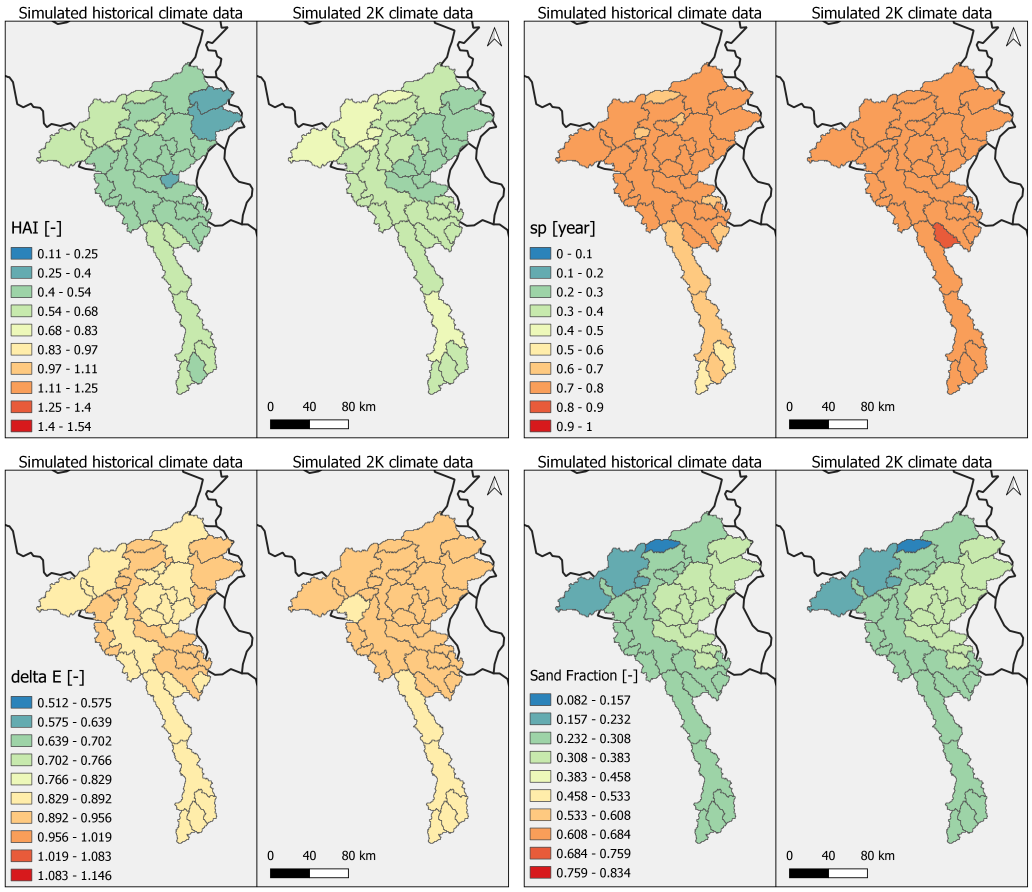

Figure 5.9: The values of the catchment descriptors that are part of the regression analysis, for the simulated historical and 2K climate data catchments of the Meuse. The catchment descriptors are: Holdridge Aridity Index (HAI), phase shift of precipitation (s_P), seasonal amplitude for the potential evaporation (δ_E), and sand fraction (sand_frac).

Based on the PCA it is known that s_P is not strongly correlated to the root-zone storage capacity, while HAI is positively correlated, and $sand_{frac}$ and δ_E are negatively correlated. This means that the highest root-zone storage capacity values are found in areas with high HAI and low δ_E and $sand_{frac}$ values. Figure 5.9 shows the variable values for the simulated historical and 2K climate data of the Meuse catchments. Comparing the simulated historical and 2k climate data results in differences for HAI, s_P, and δ_E that range between 0.08-0.12, 0.02-0.21 year, and -0.01-0.01

respectively. The change in δ_E is small, which has limited impact on the root-zone storage capacity. The increase in HAI results in an increase of the root-zone storage capacity. The increase of s_P results in a decrease of the root-zone storage capacity. $sand_{frac}$ does not impact the root-zone storage capacity as it remains constant. Since the HAI has a stronger correlation to the root-zone storage capacity compared to s_P, the root-zone storage capacity is expected to increase as a result of the simulated 2K warming climate data. The variable values for each of the selected catchments are shown in Figure 5.10. The current catchments that have the most similar variable values compared to the simulated 2K climate data catchments are outlined with purple. These catchments are found in the Southern part of Great-Britain.

To estimate the root-zone storage capacity, the regression relationship has been applied to the catchments. To estimate the regression coefficients for each of the catchments, the regression model with cross-validation has been iterated 1000 times using the independent variables that have been selected. Each iteration results in different regression coefficients. These coefficients have then been used to estimate the root-zone storage capacity of the catchments in question. For each catchment 1000 different root-zone storage capacities are computed. The median of these values is the root-zone storage capacity that is assigned to the catchment.

This regression relationship is used to estimate the root-zone storage capacity for the simulated historical climate data Sr-Hist$_{\mathrm{RM}}$ and the simulated 2K climate data Sr-2K$_{\mathrm{RM}}$ of the Meuse catchments. The resulting root-zone storage capacity values are given in Appendix D.

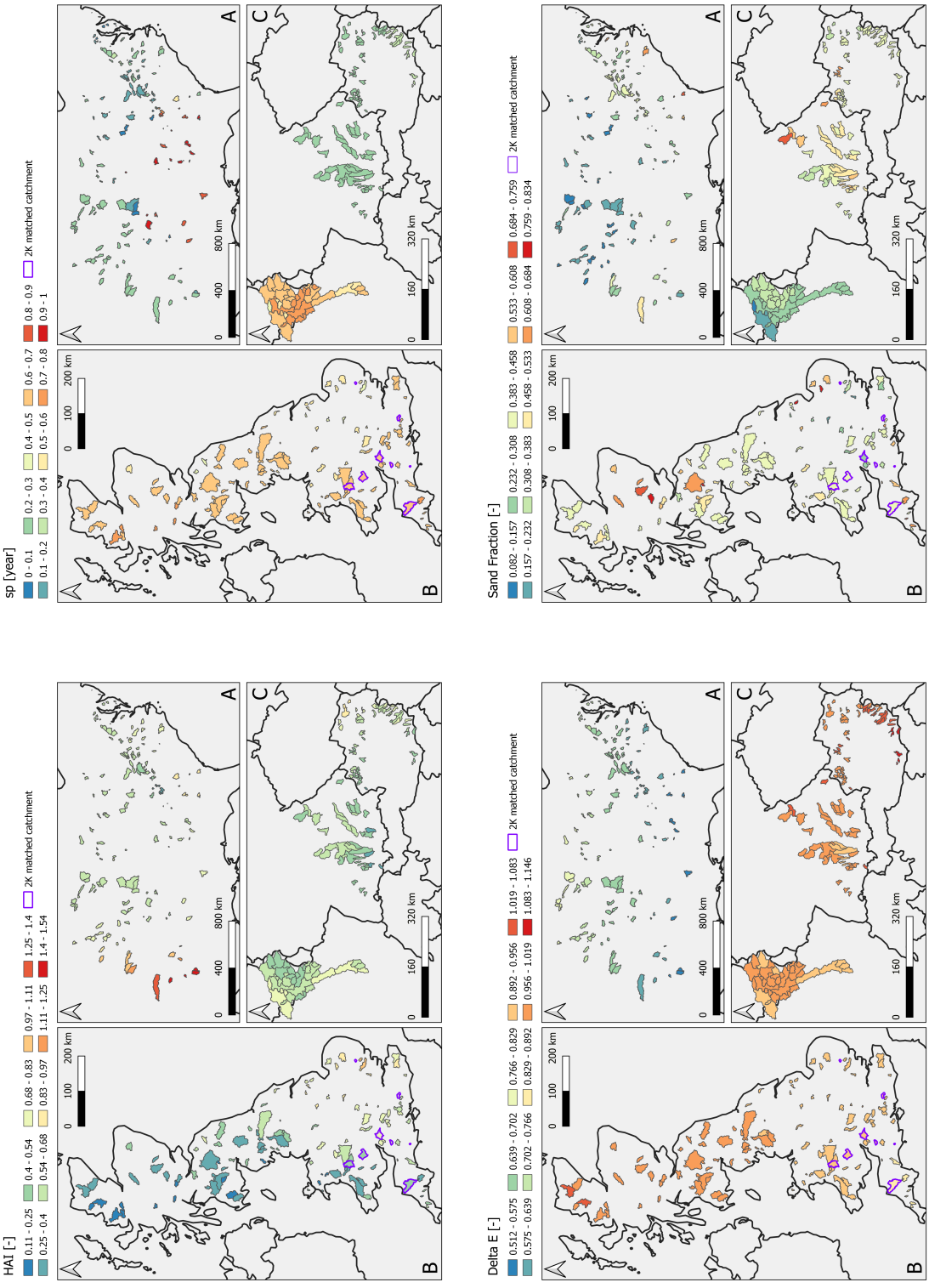

Figure 5.10: The values of the catchment descriptors that are part of the regression analysis, for each of the selected catchments. The catchment descriptors are: Holdridge Aridity Index (HAI), phase shift of precipitation (s_P), seasonal amplitude for the potential evaporation (δ_E), and sand fraction (sand_frac).

5.3 Comparison of the root-zone storage capacity methods

The root-zone storage capacities of the Meuse catchments have been estimated for the simulated historical and future 2K warming conditions using the water balance method and the regression relationship. In this study these root-zone storage capacities are distinguished using the following abbreviations: Sr-Hist$_{WB}$ is used for the S_r calculated for the simulated historical climate data using the water balance method. Sr-Hist$_{RM}$ is used for the S_r estimated for the simulated historical climate data using the regression relationship and Sr-2K$_{RM}$ is used for the S_r estimated for the simulated 2K climate data using the regression relationship. The exact magnitudes of these different S_r estimates for each of the Meuse catchments have been provided in Appendix D.

The regression method has been calibrated using S_r values that were computed with the water balance method. Since the regression model is not perfect there remains a difference between Sr-Hist$_{WB}$ and Sr-Hist$_{RM}$ (Figure 5.11). Generally, the Sr-Hist$_{WB}$ values are larger compared to the Sr-Hist$_{RM}$ values, with four catchments showing extreme difference between the two S_r values (> 49mm). The mean error, mean absolute error, and mean absolute percentage error between the two S_r estimates are -15 mm, 25 mm, and 11.4% respectively. When ignoring the four extreme values the ME, MAE, and MAPE become -12 mm, 18 mm, and 8.5%. These values indicate that overall the regression relationship results in underestimations of the root-zone storage capacity.

The aim of the regression model is to be able to produce time-dynamic root-zone storage capacities. Therefore, the regression model is used to compute S_r for both the simulated historical (Sr-Hist$_{RM}$) and the simulated 2K climate data set (Sr-2K$_{RM}$) (Figure 5.12a,b). The values of Sr-2K$_{RM}$ are all larger compared to the Sr-Hist$_{RM}$ values, with an average increase of approximately 27 mm or 11.8%. The difference between the root-zone storage capacities is shown in Figure 5.12c. This figure shows that differences are largest in the Southern catchments, and smallest for the catchments in the Northeastern part of the river system.

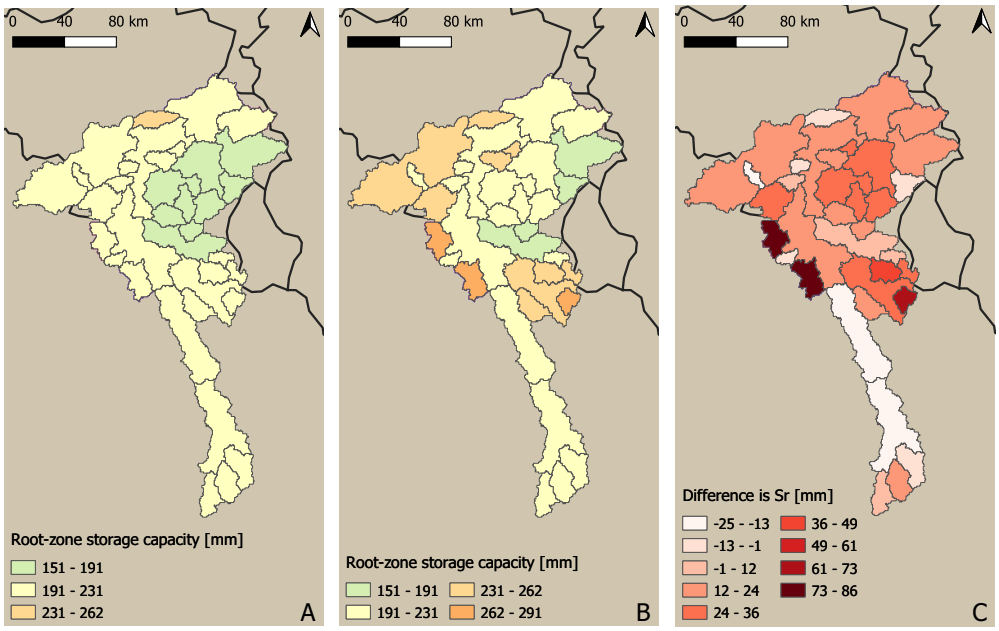

Figure 5.11: The root-zone storage capacities for the Meuse catchments (a) Sr-Hist$_{RM}$, (b) Sr-Hist$_{WB}$, and (c) the difference between Sr-Hist$_{WB}$ and Sr-Hist$_{RM}$.

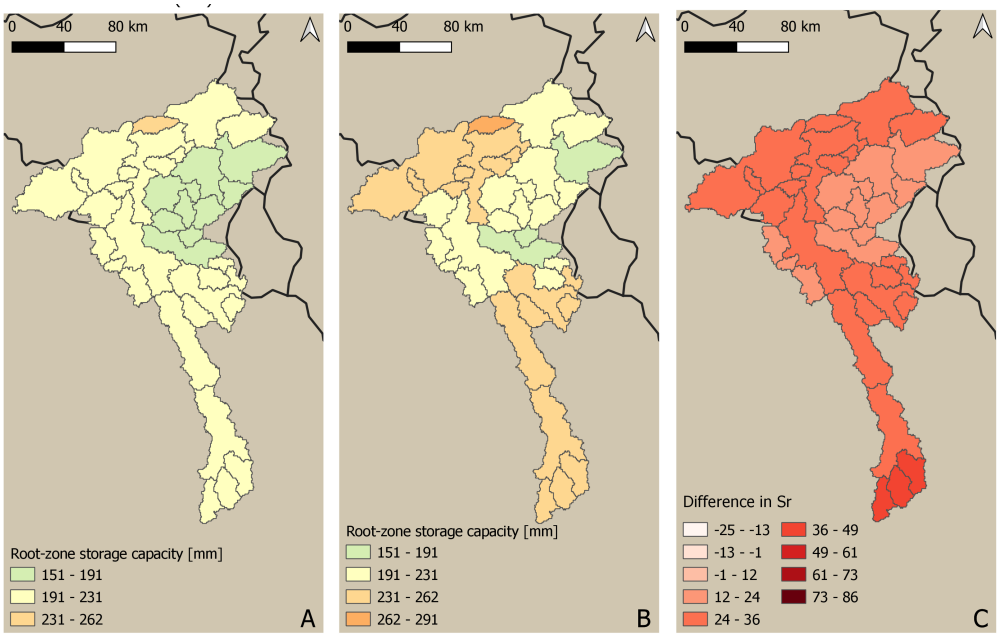

Figure 5.12: Map of the estimated root-zone storage capacities for the Meuse catchments (a) Sr-Hist$_{RM}$, (b) Sr-2K$_{RM}$, and (c) the difference between Sr-2K$_{RM}$ and Sr-Hist$_{RM}$.

5.4 Evaluation of the scenario results

5.4.1 Scenario results

As mentioned in the methodology, three different model scenarios have been considered. Each of these scenarios evaluates the difference in hydrological response between a model run forced with the historical climate simulation and a model run forced with the 2K climate simulation. The model forcings are identical for each of the scenarios, it is the root-zone storage capacity that is adjusted to describe either stationary or time-dynamic model parameters. The provided results indicate the difference in hydrological response between the 2K climate simulation and the historical climate simulation. For example, an increase in streamflow indicates that for the 2K simulation a higher streamflow has been projected relative to the projection of the historical simulation.

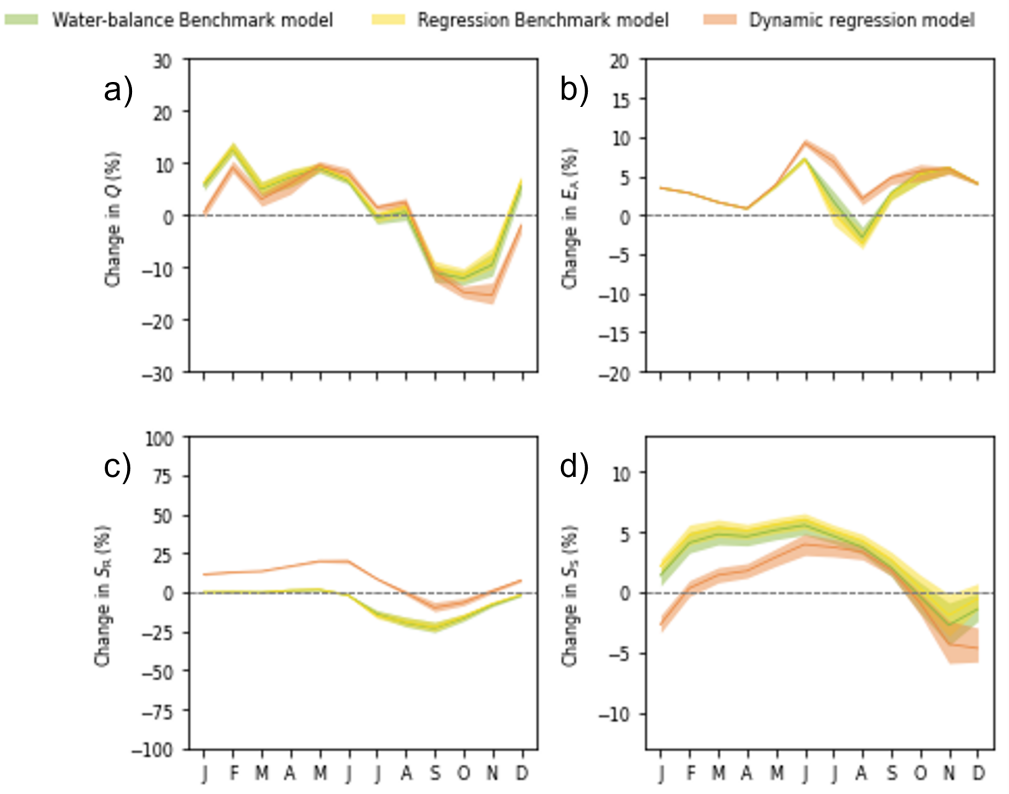

Figure 5.13: Percentage change in mean monthly hydrological response of several flux and state variables between the 2K and historical model runs for the three scenarios, each based on different assumptions for the root-zone storage capacity parameter S_r. Percentage change in mean monthly (a) streamflow Q, (b) actual evaporation E_A, (c) root-zone storage S_r, (d) groundwater storage S_s.

Scenario 1: Benchmark - Water balance method
For the first scenario Sr-Hist$_{WB}$ has been used as the root-zone storage capacity value for both the historical and the 2K climate simulation part of the model. The model uses the root-zone storage capacity as a static parameter. This scenario is called the benchmark model for the water balance method. Figure 5.13, illustrates the percentage change in mean monthly hydrological response of several flux and state variables between the 2K and historical model runs.

The projected streamflow shows an increase from December to August with an average of +5.7%. The maximum increase of approximately +12.8% is projected in February. The streamflow shows a decrease in the period between September and

November with a maximum of around -12.1% in October. The projected actual evaporation shows increased values for most of the year, with an average increase of +3.6%. The figure shows that during the spring the actual evaporation will increase as a result of the 2K climate simulation, with a maximum increase of around +7.2% in June. However, during the summer months the difference in actual evaporation between the climate scenarios decreases, with a minimum of -2.9% in August. The projected root-zone soil moisture remains similar at the start of the year, after which a slight increase is projected during April and May. During the rest of the year the root-zone soil moisture is projected to decrease with a maximum of approximately -23.1% in September. The projected groundwater storage increases the majority of the year with an average of +4.0% and a maximum of approximately +5.5% in June. A slight decrease has been projected in the period between October and December, with a maximum of -2.8%.

Scenario 2: Benchmark - Regression relationship
In the second scenario Sr-Hist$_{RM}$ has been used for both the historical and the 2K climate simulation part of the model. Similar to scenario 1, the root-zone storage capacity has also been modelled as a static parameter. This scenario is called the benchmark model for the regression relationship. Figure 5.13, illustrates the percentage change in mean monthly hydrological response of several flux and state variables between the 2K and historical model run.

The projected streamflow shows an increase from December to August with an average of +6.2%. The maximum increase of approximately +12.9% is projected in February. The streamflow shows a decrease in the period between September and November with a maximum of around -11.5% in October. The actual evaporation shows increased values for most of the year, with an average increase of +3.4%. The graph shows that during the spring the actual evaporation will increase as a result of the 2K climate simulation, with a maximum increase of approximately +7.2% projected in June. However, during the summer months the difference in actual evaporation between the scenarios decreases, with a minimum of -3.7% in August. The projected root-zone soil moisture remains similar at the start of the year, after which a slight increase is projected during April and May. During the rest of the year the root-zone soil moisture is projected to decrease with a maximum of -22.6% in September. The projected groundwater storage increases the majority of the year with an average of +4.2% and a maximum of +6.0% in June. A slight decrease has been projected in the period between October and December, with a maximum of -1.9%.

Scenario 3: Dynamic - Regression relationship
In contrast to the previous scenarios, the third scenario uses a time-dynamic root-zone storage capacity. The scenario is called the dynamic regression scenario. For the historical part of the model Sr-Hist$_{RM}$ has been used, while Sr-2K$_{RM}$ has been used for the 2K part of the model. The differences between the hydrological response between the 2K part of the model and the historical part of the model are illustrated in Figure 5.13.

The projected streamflow shows an increase from January to August with an average of +5.0%. The maximum increase of approximately +9.1% is projected in February. The streamflow shows a decrease in the period between September and December with a maximum of around -15.4% in November. The actual evaporation projects an average annual increase of +3.4%. This increase is small during the first months of the year, but reaches a maximum of +9.2% in June, after which it decreases to +2.1% in August, which is followed by higher values towards the end of the year. The projected root-zone soil moisture will increase in the first half year with an average of +12% and maximum of +19.9% in June. After which the change will decrease and reaches a minimum of -9.9% in September. The projected groundwater stor-

age shows a decrease in the winter period, with a maximum of -4.6% in December, while an average increase of +2.4% is projected during the rest of the year, with a maximum increase of +4.0% in June.

5.4.2 Comparing the scenario results

Evaluating the model results gives insight into the hydrological response of the future systems. It gives an indication of how the systems will be changing as a result of climate change. Additionally, by comparing the different scenario results the impact of the computation method and the use of a time-dynamic root-zone storage capacity can be quantified.

The impact of the computation method for S_r on the hydrological response
Scenario 1 and 2 both used the same S_r value for the historical and 2K simulation part of the model. Therefore, the only difference between these scenarios is the method which has been used to estimate the S_r values of the Meuse catchments. Comparing the scenarios indicates the impact of the estimation approach on the hydrological response of the Meuse catchments. Figure 5.13 shows that both benchmark models follow the same trends for the flux and state variables that have been discussed. The difference in projected streamflow ranges from 0.2% to 1.12%. The benchmark scenario of the regression model provides higher streamflow changes relative to the benchmark scenario of the water balance method. For the absolute evaporation, the water balance benchmark projects larger changes, ranging from 0.0% to 1.5% in July. The difference between the benchmark scenarios for the root-zone storage capacity range from 0.03% to 1.1%. Finally, the differences for the groundwater storage ranges from 0.44% to 0.87%. For both the root-zone storage and groundwater storage the benchmark model for the regression model projects higher changes. Based on these values it can be stated that the method that is used to estimate the S_r values only has a small impact on the change in hydrological response. The small differences shows that the regression method is in good agreement with the water balance method, making scenario 2 a realistic reference scenario with which the impact of the dynamic root-zone storage capacity can be identified.

The observed streamflow and the modelled streamflow of the benchmark scenarios for the historical run are plotted in Figure 5.14. This figure shows that the modelled streamflow for the historical run follows roughly the same pattern as the observed streamflow. This indicates that the Wflow_FLEX-Topo model responds correctly to the forcing data. Although the model shows the same response to the data, the difference between the modelled and observed values does indicate that there is some uncertainty in the modelled streamflow.

The impact of the time-dynamic root-zone storage capacity on the change in hydrological response
Scenario 2 and 3 both use the regression relationship to estimate the S_r values that have been used within the model runs. The difference between the scenarios lies with the fact that the second scenario uses a static S_r value, while scenario 3 adapted the S_r value to the changing climatic conditions by using a time-dynamic root-zone storage capacity. Since the estimation method remains the same, the difference between these two scenarios only represents the impact of the time-dynamic S_r value on the change in hydrological response of the Meuse catchments.

For the projected streamflow the dynamic regression model produces generally lower values compared to the benchmark model. The largest differences have been projected during the winter months, with a maximum difference of 8.6% during December. The projected actual evaporation differs between the scenarios for the summer and autumn months. The maximum difference between the scenarios has been projected in July with 6.6%. The root-zone storage capacity shows larger changes for

the dynamic regression scenario. These differences range from 8.0% in November to 23.6% in July. Finally, for the groundwater storage the differences between the scenarios are smallest during the summer month but increase to a 4.8% difference in January.

These values indicate that the use of a time-dynamic root-zone storage capacity results in an increase of absolute evaporation during the summer months, while at the same time resulting in lower values for the streamflow and groundwater storage during the winter months. The root-zone storage shows an increase throughout the whole year. In other words, the time-dynamic root-zone storage capacity has a significant impact on the seasonality of the change in the hydrological response.

Figure 5.15 shows the modelled streamflow for the 2K run of the benchmark scenarios and the dynamic regression scenario. This figure shows that all the modelled streamflows follow the same pattern. During the summer months, the streamflow is the same for all model scenarios. In the winter months, the streamflow of the dynamic regression run is slightly less compared to the benchmark models.

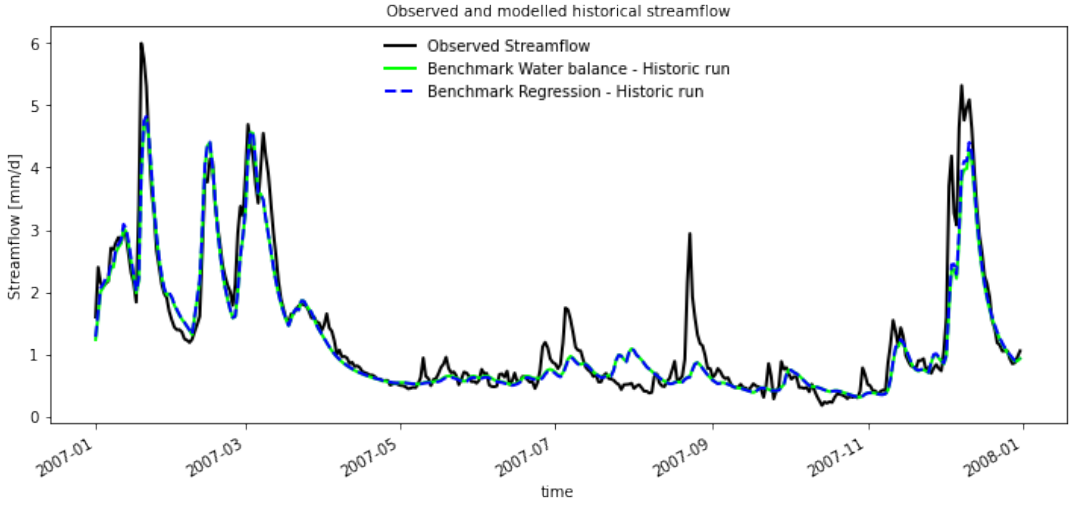

Figure 5.14: The observed streamflow for 2007 and the modelled historical streamflow of both benchmark scenarios for 2007.

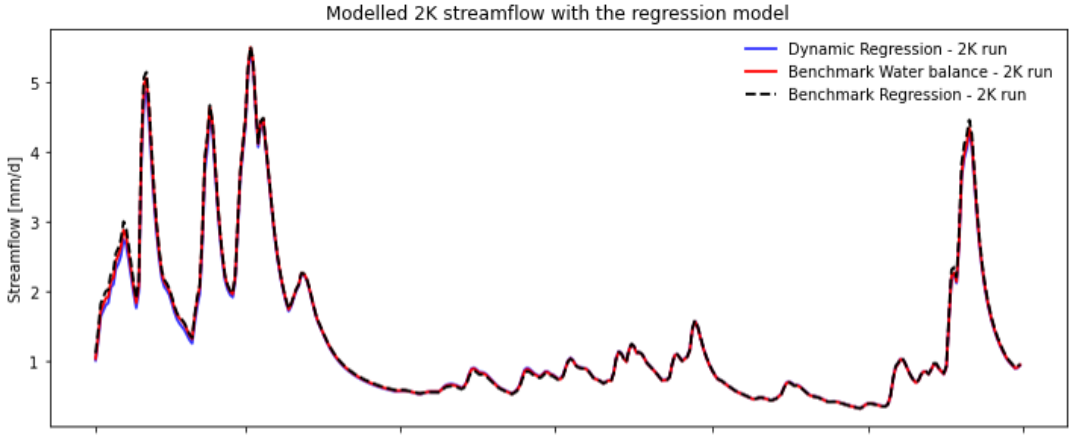

Figure 5.15: The modelled streamflow for the 2K run of each scenario.

6 | Discussion

This chapter discusses the main assumptions of the study and how they might have affected the results. First the data sets are discussed (Section 6.1), after which we highlight the water balance and regression method (Section 6.2 and 6.3). Two strong assumptions that have been made in this study are discussed in the study implications (Section 6.4). Finally, the wider application of this research is described in Section 6.5.

6.1 Data uncertainty

The data sets described in Section 3 have been used in different ways throughout this study. Errors in these data sources can have affected the computed root-zone storage capacities. For hydrological data the uncertainty magnitudes are typically in the range 10-40%. This uncertainty can be caused by measurements, derived data, interpolation, scaling, and data management uncertainty (McMillan et al., 2018). Large sample data sets are often created by combining different data sources into one large data set. During the assembly process the data is vigorously checked to ensure the quality of the data. For this study additional requirements have been set to the data, to make sure that the compared data is influenced by the same processes. Therefore, both catchments with large human and/or snow impact have been excluded from this research. Although these measures have been taken, the reader should remain aware that there will always be some uncertainty resulting from the use of data sets. More information regarding the uncertainty of the different data sets can be found in the respective documentation as mentioned in Section 3.2.

One source of data uncertainty that must be discussed in more detail, is the uncertainty related to the estimation of the potential evaporation. As mentioned in Section 3.2.4, most of the data sets used different methods to estimate the potential evaporation in the catchments. The simulated climate data used the Makkink equation for the Meuse catchments, while the Priestly-Taylor equation was used by CAMELS-USA, and both CAMELS-GB and LamaH for Central Europe used the FAO Penman-Monteith equation. In order to compare the data accurately the method in which the potential evaporation has been estimated should be the same for each of the data sets. Therefore, the Makkink equation has been used to estimate the potential evaporation in the majority of the data sets. The Makkink equation estimates the potential evaporation solely on the temperature and the incoming short-wave radiation data. However, relative humidity, wind and other factors also play a role when it comes to the potential evaporation. Therefore, this method introduces an uncertainty to the potential evaporation values.

Section 3.2.4 describes how the Makkink equation has been applied to CAMELS-USA and CAMELS-GB. Due to this new method the mean daily potential evaporation of the selected CAMELS-USA catchments have decreased with -0.03 to -1.08 mm day^{-1}, depending on the catchment. The mean daily potential evaporation of the selected CAMELS-GB catchments increased with +0.02 to +0.25 mm day^{-1}, depending on the catchment. Since both the CAMELS-GB and CAMELS-USA data set

have been created with the use of a different potential evaporation equation, applying the Makkink equation will have a slight impact on the accuracy of the data set. The LamaH catchments did not contain data for the incoming shortwave radiation, making it difficult to apply the Makkink equation to this data set. An attempt has been made to determine a correction factor based on the changes in potential evaporation of the CAMELS-GB data set, since this data set used the same approach of computing the potential evaporation as the LamaH data set. However, based on the computed changes in potential evaporation no correction factor could be derived. The decision was made to use the LamaH catchments with the provided estimates of the potential evaporation. Applying the Makkink equation to the majority of the catchments, decreased the uncertainty drastically, however a part of this uncertainty remains as the potential evaporation of the LamaH catchment could not be derived with this method.

6.2 The water balance method

The water balance method is based on the assumption that the root-zone storage capacity can be derived from the maximum annual water deficits caused by the difference between the cumulative daily precipitation and transpiration. The daily precipitation and transpiration values have been determined based on the hydrological data which comes with its uncertainty as discussed in the previous section. Since transpiration is too complex to measure at the catchment scale, this parameter has been determined based on the long-term water balance. Daily potential evaporation rates have been used to scale the data and create daily transpiration values. This method retains the seasonality of transpiration without violating the long-term mean transpiration amounts. However, this method excludes any extreme events and potential inter-annual variability in the transpiration. Hydrological events during which the water availability is limited or abundant are therefore not present in the transpiration data. This lack of inter-annual variability introduces an uncertainty within the water balance method. The impact of this uncertainty is difficult to quantify, since the values cannot be compared to real world transpiration data.

Moreover, this research has neglected the presence of interception when using the water balance method. The absence of interception causes all precipitation to enter the soil meaning less water will be available for transpiration, resulting in an underestimation of the storage deficits. However, Bouaziz et al. (2020) states that the magnitude of the fluctuations due to interception are minor relative to the magnitude of the storage deficits. Based on this research, it is believed that the assumption of no interception will not have a significant impact on the results of this study.

Since interception has been neglected, the water balance method implicitly assumes that all precipitation immediately infiltrates into the root-zone. This assumption neglects other processes such as Infiltration Excess Overland Flow and Saturation Excess Overland Flow (Stewart et al., 2019). Infiltration Excess Overland Flow occurs when the water input exceeds the infiltration rate of the soil. This might occur during periods of extreme precipitation. The water that is not able to enter the soil will be routed towards different areas. Saturation Excess Overland Flow occurs when soil pores of the unsaturated zone are completely filled, making the pores saturated, which also results in overland flow. Both of these processes indicate a high volume of water that wants to or has already entered the system. These processes will therefore not occur in times of water deficits. Therefore, the absence of these processes in the water balance method are unlikely to impact the estimates of the root-zone storage capacities.

Different ecosystems have evolved different strategies to survive droughts of different return periods. Vegetation like grasslands, shrublands, croplands, and barren or sparsely vegetated lands survive extreme droughts by going dormant (Brunner et

al., 2015). Therefore, the root-zone storage capacity of these vegetation types are adapted to the droughts of average years. Which means that the S_r for these vegetation types can be computed using short return periods. Forests on the other hand are adapting their root-zone storage capacity for extreme years. The S_r for these vegetation types should be computed using longer return periods (Wang-Erlandsson et al., 2016). For this research the choice has been made to use a return period of 20 years for all catchments. This choice will have likely resulted in an overestimation of the root-zone storage capacity in the areas with high percentages of low vegetation.

6.3 The regression relationship

In this study Multi-Linear Regression analysis has been applied to a selection of catchment descriptors, in order to obtain a regression relationship which can predict the time-dynamic root-zone storage capacity. The multi-linear regression that is used in this study is a conditional mean of the root-zone storage capacity given a selection of catchment descriptors. This regression relationship has a specific functional form. Another approach to find a relationship between the root-zone storage capacity and the catchment descriptors can be found by using a joint distribution. This approach does not assume a specific functional form between the root-zone storage capacity and the catchment descriptors, but the relationship is governed by the choice of the distribution. Additional research can be done to determine whether such an approach would provide a relationship with higher predictive powers.

The regression relationship that has been selected and used in this study has an adjusted R^2 value of approximately 0.70. This value indicates that although there is a linear relationship between the catchment descriptors and the root-zone storage capacity, this relationship is not perfect. The imperfectness of the relationship introduces an uncertainty for the root-zone storage capacities that have been estimated with this method. The results show that, for the Meuse catchments, the regression model deviates from the water balance method with approximately 11%.

There might be ways in which the regression relationship can be improved. Currently, it is believed that the selected relationship is the best relationship that can be created based on the catchment descriptors that have been used in this study. The knowledge about the root-zone storage capacity and what processes influence this parameter is still evolving. Chances are that there are descriptors that have not been considered in this study, that would result in a better performing regression relationship.

The regression relationship itself has been created to best predict the root-zone storage capacity of the Meuse catchments. The large sample data sets that have been used, contain catchments close to the climate conditions of the current and future Meuse catchments. This gives an indication of how the root-zone storage capacities will change under these conditions. However, there is still a difference between the variable values of the catchments that were matched to the Meuse catchments of the simulated 2K climate data as shown in Section 5.2.5. Especially the δ_E value is not matched perfectly. The limited availability of large sample data sets might be the reason for these results. The climate zones in the Northern Hemisphere are expected to shift northwards as a consequence of climate change. This means that the current climate conditions of France are expected to be the closest match with the future Meuse climate. Therefore, adding a France data set to the regression would probably result in more accurate estimates for the dynamic root-zone storage capacity. The CAMELS-FR data set that has been created in the past year might be a good addition.

The objective of this study is to propose a method with which dynamic root-zone storage capacities can be computed in order to predict the change in hydrological response of the Meuse catchments as a result of climate change. Although the re-

sults of the regression relationship might not be perfect, they can be used for this purpose. The difference between the benchmark scenarios show that the use of the regression relationship only has a small impact on the projected change compared to the use of the water balance method. Thereby, validating the regression relationship as a way to estimate the dynamic root-zone storage capacities for hydrological climate modelling purposes.

Bouaziz et al. (2021) studied the change in root-zone storage capacity as a result of climate change, by shifting the catchments within the Budyko framework. This approach resulted in an increase of +34% for the future root-zone storage capacity, this is a relatively large increase compared to the +11.8% that was found in this study. This indicates that the approach with which the root-zone storage capacity is estimated, has a large impact on the root-zone storage capacity values. Additional research to increase our understanding of the impact that climate change has on the root-zone storage capacity might provide more information regarding the accuracy of these estimated changes.

The magnitude of uncertainty that is introduced by the Wflow_FLEX-Topo model is outside the scope of this study.

6.4 Study implications

There are two major assumptions and unknowns that have not yet been highlighted in this discussion. These assumptions have to do with the principles that underline this entire research. First of all, the regression relationship has been derived with the use of climate analogy. This means that in theory, the root-zone storage capacities of the 2K Meuse catchments are matched to the root-zone storage capacities of current regions with similar catchment descriptors. This implies that the vegetation that is currently present in the matched region, is similar to the vegetation of the future Meuse basin. However, it is unknown whether the vegetation of the Meuse basin will be able to adapt to climate change so that the effect that it has on the hydrology will eventually resemble the effect of the vegetation in the matched region. Assuming that the vegetation will be able to adapt in the same way, it remains uncertain how long this adaption will take. This includes adaptations of individual plants, such as different water-use efficiency and root-systems but also actual changes of the vegetation community as a whole from the combination of species that are currently present to a completely new combination of (better adapted) species.

The previous reasoning assumes that there is no human disturbance in the catchments. However, in reality there are always human disturbances, especially in the Meuse basin. Therefore, the assumption that the vegetation will reach a natural equilibrium is rather implausible. Instead human interactions might alter the Meuse basin, for example by planting species or using the land. The water balance derived estimates of the root-zone storage capacity implicitly includes these effects, for the specific locations for which these estimates are computed. When transferring the root-zone storage capacity following the regression relationship to the 2K Meuse basin, the indirect assumption is that the humans will interfere with vegetation in the same way as they currently do in the matched region.

The unknowns related to the way in which vegetation will adapt and how humans will interfere with the natural conditions, create a large uncertainty in the results of this research. These uncertainties should be kept in mind when discussing the wider applications of this study. Additional research should be done to investigate the validity of these assumptions.

6.5 Wider application

The regression relationship that is proposed in this study has been specifically created for the Meuse basin. The catchments that were part of the analysis were mainly located in temperate climate zones. Therefore, this relationship might be suitable for locations within the temperate climate zones, but it is unsure if reliable estimation can be made for locations without a temperate climate.

This study indicates that the use of a time-dynamic root-zone storage capacity, has a significant impact on the change in hydrological response of the Meuse catchments, under 2K global warming conditions. The results show a large increase in seasonality with the time-dynamic S_r values. This increase is important for water management as it might result in water shortages during the summer months. Therefore, especially for long-term climate predictions, the use of a time-dynamic root-zone storage capacity should be incorporated into the hydrological models. However, the proposed method is subject to uncertainties, as comparing the results from the regression relationship with the water balance method, resulted in a mean absolute percentage error of approximately 11%. The results of the regression relationship are promising and suggest that it might be a good way to estimate the root-zone storage capacity for climate projections. However, for the direct implementation of this relationship into hydrological models, a decrease in the error with the water balance would be favorable. Therefore, further research must be done to create a better understanding about the processes that influence the root-zone storage capacity. As this might result in new catchment descriptors that produce better performing models. Current hydrological models might already benefit from the use of the water balance method to estimate the root-zone storage capacity, instead of calibrating the parameter, as this method is more reliable then the calibration.

7 | Conclusion and recommendations

The use of non-stationary root-zone storage capacities has been recognized as an important step towards more accurate hydrological models. This study proposes a regression relationship to estimate the root-zone storage capacity of the Meuse catchments for historical and future 2K warming conditions. This method is based on climate analogy mapping, which matches the root-zone storage capacities of the Meuse for simulated 2K climate data to the root-zone storage capacities of current regions with similar catchment descriptors. Based on this principle a regression relationship has been derived, that estimates the root-zone storage capacity based on the following catchment characteristics: Holdridge Aridity Index (HAI), phase shift of precipitation (s_P), seasonal amplitude for the potential evaporation (δ_E), and sand fraction (sand_frac) (Equation 7.1).

$$S_r = \beta_0 + \beta_{HAI} * HAI + \beta_{s_P} * s_P + \beta_{\delta_E} * \delta_E + \beta_{sand_{frac}} * sand_{frac} \tag{7.1}$$

This regression relationship has an adjusted R^2 value of approximately 0.70 and a mean error of 25 mm compared to the values that were computed with the water balance method for the simulated historical climate data of the Meuse catchments. Further research into the processes that influence the root-zone storage capacity and the addition of additional catchment might increase the accuracy of the regression relationship.

The impact of the regression relationship on the hydrological response of the Meuse catchments under change, has been quantified with the use of the Wflow_FLEX-Topo model. Three model scenarios were identified and each model scenario consisted of two parts, namely a historical and a 2K model run. The benchmark models use the same root-zone storage capacity for both parts of the model, in other words the root-zone storage capacity is a static parameter in these scenarios. Comparing the benchmark scenario of the water balance method with the benchmark scenario of the regression relationship showed that the differences in projected changes for the streamflow, actual evaporation, root-zone moisture storage, and groundwater storage range between 0.2-1.12%, 0-1.5%, 0.03-1.1%, and 0.44-0.87%, respectively. These relatively small differences indicate that the impact of the regression relationship on the change in hydrological response is limited compared to the use of the water balance approach. This supports the conclusions that will follow for the use of a dynamic root-zone storage capacity.

The dynamic regression scenario used the regression relationship to estimate the root-zone storage capacity for the simulated historical climate data and used these estimations for the historical part of the model. The regression relationship was also used to estimate the root-zone storage capacities for the simulated 2K climate data. These values were used for the 2K part of the model. Comparing the dynamic regression scenario to the regression benchmark scenario indicates that the

implementation of the time-dynamic root-zone storage capacity, results in changes in mean monthly hydrological response for the streamflow, actual evaporation, root-zone moisture storage, and groundwater storage with maximum -8.6%, +6.6%, +23.6%, and -4.8%, respectively. These values indicate that the use of a time-dynamic root-zone storage capacity results in an increase of absolute evaporation during the summer months, while at the same time resulting in lower values for the streamflow and groundwater storage during the winter months. The root-zone storage capacity shows an increase throughout the whole year. In other words, the time-dynamic root-zone storage capacity has a significant impact on the seasonality of the change in the hydrological response.

The changes in hydrological response with the use of a time-dynamic root-zone storage capacity, indicate the importance of implementation of time-dynamic parameters into hydrological models. Especially for long-term climate predictions a time-dynamic root-zone storage capacity can largely impact the model outcomes. The results of the regression relationship are promising and suggest that it might be a good way to estimate the root-zone storage capacity for climate projections in temperate climates. However, for the direct implementation of this relationship into hydrological models, a decrease in the error with the water balance would be favorable. Therefore, further research must be done to create a better understanding about the processes that influence the root-zone storage capacity. Current hydrological models might already benefit from the use of the water balance method to estimate the root-zone storage capacity, as this method is based on hydrological data, resulting in more accurate values compared to the calibration approach.

References

Aalbers, E. E., Lenderink, G., van Meijgaard, E., & van den Hurk, B. J. (2018). Local-scale changes in mean and heavy precipitation in western europe, climate change or internal variability? Climate Dynamics, 50(11), 4745–4766.

Aalbers, E. E., van Meijgaard, E., Lenderink, G., de Vries, H., Haarsma, R., & van den Hurk, B. (2019). The 2018 european drought under future climate conditions. In Agu fall meeting abstracts (Vol. 2019, pp. H12F–06).

Addor, N., Newman, A. J., Mizukami, N., & Clark, M. P. (2017). The camels data set: catchment attributes and meteorology for large-sample studies. Hydrology and Earth System Sciences, 21(10), 5293–5313.

Agency, E. E. (2020). Corine land cover (clc) 2018 version 2020_20u1. (Accessed 27 June 2021). Available at: https://land. copernicus. eu/pan-european/corine-land-cover/clc2018? tab= download.

Alexopoulos, E. C. (2010). Introduction to multivariate regression analysis. Hippokratia, 14(Suppl 1), 23.

Allen, R. G., Pereira, L. S., Raes, D., Smith, M., et al. (1998). Crop evapotranspiration-guidelines for computing crop water requirements-fao irrigation and drainage paper 56. Fao, Rome, 300(9), D05109.

Berghuijs, W. R., Sivapalan, M., Woods, R. A., & Savenije, H. H. (2014). Patterns of similarity of seasonal water balances: A window into streamflow variability over a range of time scales. Water Resources Research, 50(7), 5638–5661.

Berghuijs, W. R., & Woods, R. A. (2016). A simple framework to quantitatively describe monthly precipitation and temperature climatology. International Journal of Climatology, 36(9), 3161–3174.

Berrar, D. (2019). Cross-validation.

Bouaziz, L. J., Aalbers, E. E., Weerts, A. H., Hegnauer, M., Buiteveld, H., Lammersen, R., … Hrachowitz, M. (2021). The importance of ecosystem adaptation on hydrological model predictions in response to climate change. Hydrology and Earth System Sciences Discussions, 1–39.

Bouaziz, L. J., Steele-Dunne, S. C., Schellekens, J., Weerts, A. H., Stam, J., Sprokkereef, E., … Hrachowitz, M. (2020). Improved understanding of the link between catchment-scale vegetation accessible storage and satellite-derived soil water index. Water Resources Research, 56(3), e2019WR026365.

Brunner, I., Herzog, C., Dawes, M. A., Arend, M., & Sperisen, C. (2015). How tree roots respond to drought. Frontiers in plant science, 6, 547.

Chen, W.-B., & Liu, W.-C. (2015). Water quality modeling in reservoirs using multivariate linear regression and two neural network models. Advances in Artificial Neural Systems, 2015.

Cornes, R. C., van der Schrier, G., van den Besselaar, E. J., & Jones, P. D. (2018). An ensemble version of the e-obs temperature and precipitation data sets. Journal of Geophysical Research: Atmospheres, 123(17), 9391–9409.

Coxon, G., Addor, N., Bloomfield, J. P., Freer, J., Fry, M., Hannaford, J., … others (2020). Camels-gb: Hydrometeorological time series and landscape attributes for 671 catchments in great britain. Earth System Science Data, 12(4), 2459–2483.

de Boer, T. (2017). Added value of distribution in rainfall-runoff models for the meuse basin (Doctoral dissertation, Delft University of Technology). doi: 10.4233/uuid:89a78ae9-7ffb-4260-b25d-698854210fa8

de Boer-Euser, T., McMillan, H. K., Hrachowitz, M., Winsemius, H. C., & Savenije, H. H. (2016). Influence of soil and climate on root zone storage capacity. Water Resources Research, 52(3), 2009–2024.

de Boer-Euser, T., Meriö, L.-J., & Marttila, H. (2019). Understanding variability in root zone storage capacity in boreal regions. Hydrology and Earth System Sciences, 23(1), 125–138.

de Wit, M., Peeters, H., Gastaud, P., Dewil, P., Maeghe, K., & Baumgart, J. (2007). Floods in the meuse basin: Event descriptions and an international view on ongoing measures. International Journal of River Basin Management, 5(4), 279–292.

de Wit, M., van den Hurk, B., Warmerdam, P., Torfs, P., Roulin, E., & van Deursen, W. (2007). Impact of climate change on low-flows in the river meuse. Climatic change, 82(3), 351–372.

de Wit, M., Van Den Hurk, B., Warmerdam, P., Torfs, P., Roulin, E., & Van Deursen, W. (2007). Impact of climate change on low-flows in the river meuse. Climatic change, 82(3), 351–372.

Dixon, H., Hannaford, J., & Fry, M. J. (2013). The effective management of national hydrometric data: experiences from the united kingdom. Hydrological Sciences Journal, 58(7), 1383–1399.

Falcone, J. A. (2011). Gages-ii: Geospatial attributes of gages for evaluating streamflow (Tech. Rep.). US Geological Survey.

Falcone, J. A., Carlisle, D. M., Wolock, D. M., & Meador, M. R. (2010). Gages: A stream gage database for evaluating natural and altered flow conditions in the conterminous united states: Ecological archives e091-045. Ecology, 91(2), 621–621.

Farr, T. G., Rosen, P. A., Caro, E., Crippen, R., Duren, R., Hensley, S., … others (2007). The shuttle radar topography mission. Reviews of geophysics, 45(2).

Fenicia, F., Savenije, H., Matgen, P., & Pfister, L. (2006). Is the groundwater reservoir linear? learning from data in hydrological modelling. Hydrology and Earth System Sciences, 10(1), 139–150.

Fitzgerald, J. B. (2019). Equifinality and pathways to environmental concern: A fuzzy-set analysis. Socius, 5, 2378023119872412.

Fitzpatrick, M. C., & Dunn, R. R. (2019). Contemporary climatic analogs for 540 north american urban areas in the late 21st century. Nature communications, 10(1), 1–7.

Gao, H., Hrachowitz, M., Schymanski, S., Fenicia, F., Sriwongsitanon, N., & Savenije, H. (2014). Climate controls how ecosystems size the root zone storage capacity at catchment scale. Geophysical Research Letters, 41(22), 7916–7923.

Gharari, S., Hrachowitz, M., Fenicia, F., & Savenije, H. (2011). Hydrological landscape classification: investigating the performance of hand based landscape classifications in a central european meso-scale catchment. Hydrology and Earth System Sciences, 15(11), 3275–3291.

Guhathakurta, P., & Saji, E. (2013). Detecting changes in rainfall pattern and seasonality index vis-à-vis increasing water scarcity in maharashtra. Journal of Earth System Science, 122(3), 639–649.

HANNAFORD, J. (2004). Development of a strategic data management system for a national hydrological database, the uk national river flow archive. In Hydroinformatics: (in 2 volumes, with cd-rom) (pp. 637–644). World Scientific.

Hengl, T., Mendes de Jesus, J., Heuvelink, G. B., Ruiperez Gonzalez, M., Kilibarda, M., Blagotić, A., ... others (2017). Soilgrids250m: Global gridded soil information based on machine learning. PLoS one, 12(2), e0169748.

Hennermann, K., & Guillory, A. (2020). Era5: uncertainty estimation. CDS dataset documentation, European Centre for Medium-Range Weather Forecasts (ECMWF), available at, 790.

Hersbach, H., Bell, B., Berrisford, P., Hirahara, S., Horányi, A., Muñoz-Sabater, J., ... others (2020). The era5 global reanalysis. Quarterly Journal of the Royal Meteorological Society, 146(730), 1999–2049.

Hiederer, R. (2013). Mapping soil typologies—spatial decision support applied to european soil database. EUR25932EN Scientific and Technical Research Series, 1831–9424.

Hiemstra, P., & Sluiter, R. (2011). Interpolation of makkink evaporation in the netherlands.

Hooghart, J., & Lablans, W. (1988). Van penman naar makkink: een nieuwe berekeningswijze voor de klimatologische verdampingsgetallen. De Bilt, Royal Netherlands Meteorological Institute (KNMI), De Bilt, the Netherlands, 745.

Hough, M., & Jones, R. (1997). The united kingdom meteorological office rainfall and evaporation calculation system: Morecs version 2.0-an overview. Hydrology and Earth System Sciences, 1(2), 227–239.

Hrachowitz, M., Stockinger, M., Coenders-Gerrits, M., van der Ent, R., Bogena, H., Lücke, A., & Stumpp, C. (2020). Deforestation reduces the vegetation-accessible water storage in the unsaturated soil and affects catchment travel time distributions and young water fractions. Hydrol. Earth Syst. Sci. Discuss.[preprint], https://doi. org/10.5194/hess-2020-293, in review.

Jin, S., Yang, L., Danielson, P., Homer, C., Fry, J., & Xian, G. (2013). A comprehensive change detection method for updating the national land cover database to circa 2011. Remote Sensing of Environment, 132, 159–175.

Keller, V., Tanguy, M., Prosdocimi, I., Terry, J., Hitt, O., Cole, S., ... Dixon, H. (2015). Ceh-gear: 1 km resolution daily and monthly areal rainfall estimates for the uk for hydrological and other applications. Earth System Science Data, 7(1), 143–155.

Klingler, C., Schulz, K., & Herrnegger, M. (2021). Lamah| large-sample data for hydrology and environmental sciences for central europe. Earth System Science Data Discussions, 1–46.

Lins, H. F. (2012). Usgs hydro-climatic data network 2009 (hcdn-2009). US Geological Survey Fact Sheet, 3047(4).

MacQueen, J., et al. (1967). Some methods for classification and analysis of multivariate observations. In Proceedings of the fifth berkeley symposium on mathematical statistics and probability (Vol. 1, pp. 281–297).

Marx, A., Kumar, R., Thober, S., Rakovec, O., Wanders, N., Zink, M., ... Samaniego, L. (2018). Climate change alters low flows in europe under global warming of 1.5, 2, and 3 c. Hydrology and Earth System Sciences, 22(2), 1017–1032.

McMillan, H. K., Westerberg, I. K., & Krueger, T. (2018). Hydrological data uncertainty and its implications. Wiley Interdisciplinary Reviews: Water, 5(6), e1319.

Miller, D. A., & White, R. A. (1998). A conterminous united states multilayer soil characteristics dataset for regional climate and hydrology modeling. Earth interactions, 2(2), 1–26.

Milly, P. C., Betancourt, J., Falkenmark, M., Hirsch, R. M., Kundzewicz, Z. W., Lettenmaier, D. P., & Stouffer, R. J. (2008). Stationarity is dead: whither water management? Science, 319(5863), 573–574.

Morris, D., Flavin, R., & Moore, R. (1990). A digital terrain model for hydrology.

Muchan, K., & Dixon, H. (2014). Ensuring hydrometric data are fit-forpurpose through a national service level agreement. Hydrology in a changing world: environmental and human dimensions, edited by: Daniell, TM, 323–329.

Muñoz-Sabater, J., Dutra, E., Agustí-Panareda, A., Albergel, C., Arduini, G., Balsamo, G., … others (2021). Era5-land: A state-of-the-art global reanalysis dataset for land applications. Earth System Science Data, 13(9), 4349–4383.

Newman, A., Clark, M., Sampson, K., Wood, A., Hay, L., Bock, A., … others (2015). Development of a large-sample watershed-scale hydrometeorological data set for the contiguous usa: data set characteristics and assessment of regional variability in hydrologic model performance. Hydrology and Earth System Sciences, 19(1), 209–223.

Nijzink, R., Hutton, C., Pechlivanidis, I., Capell, R., Arheimer, B., Freer, J., … others (2016). The evolution of root-zone moisture capacities after deforestation: a step towards hydrological predictions under change? Hydrology and Earth System Sciences, 20(12), 4775–4799.

Parajka, J., Blaschke, A. P., Blöschl, G., Haslinger, K., Hepp, G., Laaha, G., … Zessner, M. (2016). Uncertainty contributions to low-flow projections in austria. Hydrology and Earth System Sciences, 20(5), 2085–2101.

Pelletier, J., Broxton, P., Hazenberg, P., Zeng, X., Troch, P., Niu, G., … Gochis, D. (2016). Global 1-km gridded thickness of soil, regolith, and sedimentary deposit layers, ornl daac, oak ridge, tennessee, usa.

Pfister, L., Kwadijk, J., Musy, A., Bronstert, A., & Hoffmann, L. (2004). Climate change, land use change and runoff prediction in the rhine–meuse basins. River research and applications, 20(3), 229–241.

Refaeilzadeh, P., Tang, L., & Liu, H. (2009). Cross-validation. Encyclopedia of database systems, 5, 532–538.

Robinson, E., Blyth, E., Clark, D., Comyn-Platt, E., Finch, J., & Rudd, A. (2017). Climate hydrology and ecology research support system meteorology dataset for great britain (1961-2015)[chess-met] v1. 2.

Robinson, E. L., Blyth, E. M., Clark, D. B., Finch, J., & Rudd, A. C. (2017). Trends in atmospheric evaporative demand in great britain using high-resolution meteorological data. Hydrology and Earth System Sciences, 21(2), 1189–1224.

Rowland, C., Morton, D., Carrasco Tornero, L., McShane, G., O'Neil, A., & Wood, C. (2017). Land cover map 2015 (1km percentage aggregate class, gb).

Savenije, H. H., & Hrachowitz, M. (2017). Hess opinions catchments as meta-organisms–a new blueprint for hydrological modelling. Hydrology and Earth System Sciences, 21(2), 1107–1116.

Schär, C., Frei, C., Lüthi, D., & Davies, H. C. (1996). Surrogate climate-change scenarios for regional climate models. Geophysical Research Letters, 23(6), 669–672.

Schneider, A., Hommel, G., & Blettner, M. (2010). Linear regression analysis: part 14 of a series on evaluation of scientific publications. Deutsches Ärzteblatt International, 107(44), 776.

Shen, M., Tang, Y., Chen, J., Zhu, X., & Zheng, Y. (2011). Influences of temperature and precipitation before the growing season on spring phenology in grasslands of the central and eastern qinghai-tibetan plateau. Agricultural and Forest Meteorology, 151(12), 1711–1722.

Smith, L. I. (2002). Principal component analysis. Department of Computer Science, University Of Otago.

Stewart, R. D., Bhaskar, A. S., Parolari, A. J., Herrmann, D. L., Jian, J., Schifman, L. A., & Shuster, W. D. (2019). An analytical approach to ascertain saturation-excess versus infiltration-excess overland flow in urban and reference landscapes. Hydrological processes, 33(26), 3349–3363.

Tanguy, M., Dixon, H., Prosdocimi, I., Morris, D., & Keller, V. (2016). Gridded estimates of daily and monthly areal rainfall for the united kingdom (1890–2015)[cehgear]. NERC Environmental Information Data Centre, 10.

Thomson, N., Barrie, L., & Ayles, M. (1981). The meteorological office's rainfall and evaporation calculation system; morecs. met (Tech. Rep.). Office Hydrological Memorandum.

Uyanık, G. K., & Güler, N. (2013). A study on multiple linear regression analysis. Procedia-Social and Behavioral Sciences, 106, 234–240.

van Meijgaard, E., Van Ulft, L., Van de Berg, W., Bosveld, F., Van den Hurk, B., Lenderink, G., & Siebesma, A. (2008). The knmi regional atmospheric climate model racmo, version 2.1. KNMI De Bilt, The Netherlands.

van Voorst, L. (2020). Descriptor variables of the root zone storage capacity in canada.

Wang-Erlandsson, L., Bastiaanssen, W. G., Gao, H., Jägermeyr, J., Senay, G. B., Van Dijk, A. I., … Savenije, H. H. (2016). Global root zone storage capacity from satellite-based evaporation. Hydrology and Earth System Sciences, 20(4), 1459–1481.

Wold, S., Esbensen, K., & Geladi, P. (1987). Principal component analysis. Chemometrics and intelligent laboratory systems, 2(1-3), 37–52.

Yamazaki, D., Ikeshima, D., Sosa, J., Bates, P. D., Allen, G. H., & Pavelsky, T. M. (2019). Merit hydro: A high-resolution global hydrography map based on latest topography dataset. Water Resources Research, 55(6), 5053–5073.

Yang, X., & Giusti, M. (2020). Era5-land: data documentation. CDS dataset documentation, European Centre for Medium-Range Weather Forecasts (ECMWF), verfügbar unter: https://confluence. ecmwf. int/display/CKB/ERA5-Land% 3A+ data+ documentation (letzter Zugriff: 30.11. 2020).

A | Makkink equation

CAMELS-USA

For the CAMELS-USA data set the Makkink equation that has been used is given by Equation A.1 (Hiemstra & Sluiter, 2011).

$$ET_{ref} = 0.65 * \frac{s}{s+\gamma} \frac{K}{\lambda * \rho} \tag{A.1}$$

ET_{ref} = potential evaporation [m d^{-1}]
γ = psychrometric constant (at sea level 0.066 kPa °C^{-1})
s = the slope of the curve of saturation water vapor pressure [kPa °C^{-1}]
K = daily incoming short-wave radiation [J m^{-2} day^{-1}]
λ = Heat of vaporization of water [J kg^{-1}]
ρ = 1000 kg m^{-3} = bulk density of water

The slope of the curve of saturation water vapor pressure is calculated with:

$$slope = \frac{7.5 * 237.3}{(237.3 + T)^2} * \log 10 * e_s \tag{A.2}$$

Where e_s is the saturated vapor pressure which can be calculated with:

$$e_s = 0.6107 * 10^{\frac{7.5 * T_{Day}}{237.3 + T_{Day}}} \tag{A.3}$$

The heat of vaporization is calculated with Equation A.4 and the psychrometric constant with Equation A.5.

$$\lambda = (2501 - 2.375 * T_{Day}) * 1000 \tag{A.4}$$

$$\gamma = 0.0646 + 0.00006 * T_{Day} \tag{A.5}$$

CAMELS-GB

For the CAMELS-GB data set the incoming short-wave radiation is provided in W m^{-2} instead of in J m^{-2} day^{-1}, therefore the previous method should be adjusted to these different units. Equation A.6 will be used for the CAMELS-GB.

$$ET_{ref} = 0.65 * \frac{s}{s+\gamma} \frac{K}{\lambda} \tag{A.6}$$

ET_{ref} = potential evaporation [m d^{-1}]
γ = psychrometric constant (at sea level 0.066 kPa °C^{-1})
s = the slope of the curve of saturation water vapor pressure [kPa °C^{-1}]
K = daily incoming short-wave radiation [J m^{-2} day^{-1}]
λ = Heat of vaporization of water [J kg^{-1}]

The slope of the curve of saturation water vapor pressure is calculated with:

$$slope = \frac{abc}{(c+T)^2} * \exp \frac{bT}{c+T} \tag{A.7}$$

a = 6.1078 mbar
b = 17.294 [-]
c = 237.73 °C
T = Temperature [°C]

The heat of vaporization and the psychrometric constant have been computed in the same way as for the previous Makkink equation.

B | Python scripts

The most relevant Python scripts are published in an online repository. This repository can be accessed with the QR-code or on:

https://gitfront.io/r/user-4717306/05154cf13f200ba62c7d2d9c1d3b35ea8dd9c558/MSc-Thesis/

Figure B.1: QR-code to the Python scripts in an online repository

C | Model parameters

The symbols that are used for the fluxes of the Wflow_FLEX-Topo model are given in Table C.1. The symbols for the storage are provided in Table C.2. (Bouaziz et al., 2021)

Table C.1: Definitions of the symbols used to denote the different model fluxes (source: (Bouaziz et al., 2021))

Fluxes (mm d^{-1})	Definition
P	Precipitation
P_R	Rainfall
P_S	Snowfall
P_M	Snow melt
E_P	Potential Evaporation
E_W	Evaporation from snow storage
E_I	Evaporation from interception
E_R	Evaporation from the root-zone storage
P_E	Effective precipitation
R_R	Outflow from the root-zone storage
R_{RS}	Recharge to the slow storage
R_{RF}	Recharge to the fast storage
R_P	Percolation
R_C	Capillary rise
Q_F	Fast runoff
Q_S	Slow runoff
Q	Streamflow

Table C.2: Definitions of the symbols used to denote the different storages (source: (Bouaziz et al., 2021))

Storage (mm)	Defenition
S_W	Snow storage
S_I	Interception storage
S_R	Root-zone storage
S_F	Fast runoff storage
S_S	Slow runoff storage

D | The root-zone storage capacity of the Meuse catchments

Table D.1 shows the root-zone storage capacities of the Meuse catchments. Sr-Hist$_{\text{WB}}$ represents the S_r calculated for the simulated historical climate data using the water balance method. Sr-Hist$_{\text{RM}}$ represents the S_r estimated for the simulated historical climate data using the regression relationship. Sr-2K$_{\text{RM}}$ represents the S_r estimated for the simulated 2K climate data using the regression relationship. Besides the exact magnitudes of the different S_r estimations, the table also presents the percentage difference between Sr-Hist$_{\text{WB}}$ and Sr-Hist$_{\text{RM}}$ and between Sr-2K$_{\text{RM}}$ and Sr-Hist$_{\text{RM}}$.

Table D.1: The root-zone storage capacities of the Meuse catchments and the percentage difference between the root-zone storage capacities using different computation methods and simulated climate data.

Station	$Sr - Hist_{WB}$ **[mm]**	$Sr - Hist_{RM}$ **[mm]**	$Sr - 2KRM$ **[mm]**	**Percentage difference** $Sr - Hist_{WB}$ **and** $Sr - Hist_{RM}$	**Percentage difference** $Sr - 2K_{RM}$ **and** $Sr - Hist_{RM}$
La Meuse Goncourt	218.61	215.58	255.86	1.41	18.68
Le Mouzon Circourt-sur-Mouzon [Villars]	230.05	206.79	245.04	11.25	18.5
Le Vair Soulosse-sous-Saint-Élophe	203.7	212.54	254.87	-4.16	19.92
La Meuse Saint-Mihiel	198.15	223.36	258.76	-11.29	15.85
La Meuse Stenay	198.62	220.12	253.73	-9.77	15.27
La Bar Cheveuges	291.7	206.13	229.24	41.51	11.21
La Vence la Francheville	197.95	199.72	221.34	-0.89	10.83
La Sormonne Belval	291.7	206.13	229.24	41.51	11.21
Membre Pont	171.02	170.41	190.78	0.36	11.95
Sainte-Marie	203.93	194.42	218.89	4.89	12.59
Straimont	180.85	166.27	186.07	8.77	11.91
La Chiers Carignan	240.48	206.67	234.62	16.36	13.52
La Chiers Longlaville	140.94	214.06	246.62	-34.16	15.21
La Crusnes Pierrepont	270.1	208.12	237.8	29.78	14.26
Le Ton Étouviez	237.09	193.67	219.14	22.42	13.15
Le Loison Han-lés-Juvigny	244.19	220.57	250.57	10.71	13.6
Treignes	232.47	196.17	224.14	18.5	14.26
Chooz	215.52	202.86	229.17	6.24	12.97
Daverdisse	195.78	172.86	193.88	13.26	12.16
Jemelle	203.78	175.31	198.2	16.24	13.06
Gendron	220.64	188.98	212.96	16.75	12.69
Hastiere	226.13	222.33	252.71	1.71	13.66
Yvoir	235.0	217.64	244.99	7.98	12.57
Warnant	222.11	226.67	260.58	-2.01	14.96
Modave	237.94	213.31	240.13	11.55	12.57
Ortho	201.61	176.01	195.98	14.54	11.35
Mabompre	169.0	178.26	199.96	-5.19	12.17
Tabreux	215.38	182.42	205.24	18.07	12.51
Wiheries	204.47	219.89	247.98	-7.01	12.77
Salzinnes Ronet	240.67	225.57	254.31	6.69	12.74
Huccorgne	234.95	247.4	277.4	-5.03	12.13
Amay	223.09	205.96	231.87	8.32	12.58
Martinrive	179.61	163.28	183.9	10.0	12.63
Chaudfontaine Pisc	224.47	203.74	228.12	10.17	11.97
Maastricht	224.47	203.74	228.12	10.17	11.97

E | Boxplots for the range of catchment descriptors within each cluster

For each catchment descriptors a boxplot has been created, in which the range of this descriptor within the clusters is provided. The boxplots are given in Figure E.1.

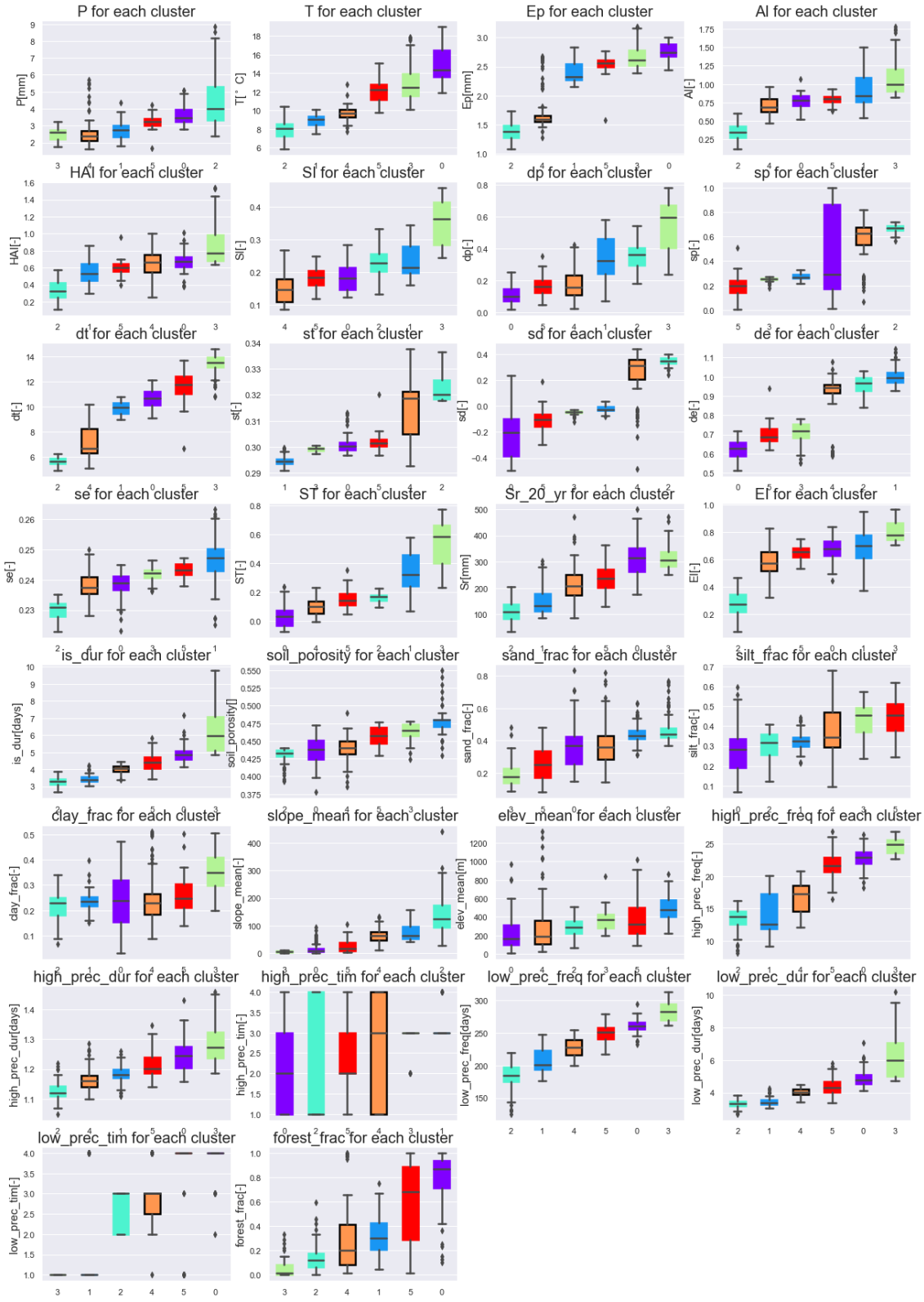

Figure E.1: Boxplots containing the range of the catchment descriptors within each cluster. The black border indicates the cluster that contains the Meuse catchments from the observed historical E-OBS data.

F | Correlating catchment descriptors

The catchment variables that are strongly correlated and the reason for the correlations are provided in Table F.1

Table F.1: The strongly correlated catchment descriptor pairs and the reason for the correlation

			Reason for correlation:
1	Ep	T	Closely related as higher temperature result in higher potential evaporation.
2	AI	HAI	Both indicate the Aridity index, but calculated differently.
3	AI	Ep	AI is computed with Ep
4	AI	P	AI is computed with P
5	HAI	P	HAI is computed with P
6	HAI	T	HAI is computed with P
7	HAI	Ep	Indirectly correlated to AI
8	SI	P	SI is computed with P
9	SI	ST	Both indicate the seasonality of precipitation
10	ST	δ_P	ST is computed with δ_P
11	ST	Δ_T	ST is computed with Δ_T
12	ST	s_P	ST is computed with s_P
13	ST	s_T	ST is computed with s_T
14	Is_dur	lpd	Practically the same descriptor
15	δ_P	P	δ_P depends on P
16	s_P	P	s_P depends on P
17	Ep	δ_E	δ_E depends on Ep
18	Ep	s_E	s_E depends on Ep
19	T	Δ_T	Δ_T depends on T
20	T	s_T	s_T depends on T
21	s_d	s_P	s_d is computed with s_P
22	s_d	s_T	s_d is computed with s_T

G | Multi-Linear Regression iteration results

This appendix contains the results of the iterations of the Multi-Linear regression. The 'param' columns show the independent variables or catchment descriptors that have been used in the regression model. The 'constant', indicates the regression coefficient of the whole line, while the 'coef'-values are the regression coefficients that correspond to the respective parameter value. For each of the models the R^2 and adjusted R^2 values of the test set have also been provided. The condition number, in the last column, indicates the multi-collinearity measured by the regression method.

Figure G.1: The best iterations for the model with 2 independent variables.

constant	param1	coef1	param2	coef2	rsquared	rsquared_adj	cond_num
271.42	HAI	261.16	de	-250.14	0.7136	0.7120	15.06
282.94	HAI	257.02	de	-263.08	0.7097	0.7081	15.19
289.02	HAI	242.68	de	-257.78	0.6850	0.6833	14.88
280.57	HAI	247.77	de	-251.87	0.6847	0.6830	14.93
272.64	HAI	249.74	de	-245.84	0.6805	0.6787	14.82
-66.85	T	28.34	low_prec_tim	-9.41	0.6608	0.6590	48.46
-82.67	T	28.44	forest_frac	-26.91	0.6531	0.6512	47.31
-79.67	T	28.43	forest_frac	-30.11	0.6450	0.6431	47.09
-67.33	T	27.89	low_prec_tim	-6.77	0.6437	0.6418	48.34
-84.37	T	29.09	forest_frac	-39.04	0.6432	0.6413	46.79
-68.07	HAI	169.40	is_dur	43.72	0.6398	0.6379	34.94
-67.58	T	28.00	low_prec_tim	-7.50	0.6375	0.6355	48.60
-78.04	T	28.77	forest_frac	-40.05	0.6351	0.6331	48.19
-78.59	T	28.59	forest_frac	-35.01	0.6308	0.6288	46.96
-19.76	HAI	342.77	forest_frac	82.71	0.6283	0.6262	7.34
-64.03	T	27.75	low_prec_tim	-7.10	0.6268	0.6248	48.60
-26.83	HAI	345.05	forest_frac	90.92	0.6256	0.6235	7.43
-66.54	HAI	165.93	is_dur	43.43	0.6198	0.6177	35.99
-54.34	HAI	160.31	is_dur	41.36	0.6065	0.6044	34.74
-52.32	HAI	153.86	is_dur	42.26	0.6063	0.6041	35.29

Figure G.2: The best iterations for the model with 3 independent variables.

constant	param1	coef1	param2	coef2	param3	coef3	rsquared	rsquared_adj	cond_num
254.76	HAI	268.67	sp	55.18	de	-265.81	0.7453	0.7432	15.80
282.70	HAI	258.23	sp	54.78	de	-288.56	0.7387	0.7365	15.90
256.03	HAI	272.30	sp	51.38	de	-266.28	0.7332	0.7310	15.64
289.02	HAI	245.71	de	-241.11	sand_frac	-48.95	0.7313	0.7291	15.90
252.84	HAI	253.41	de	-248.74	silt_frac	55.86	0.7310	0.7288	17.59
234.66	HAI	265.06	de	-222.21	forest_frac	22.50	0.7307	0.7285	21.10
264.22	HAI	264.65	de	-238.58	ST	-35.29	0.7306	0.7284	16.46
252.37	HAI	260.92	de	-239.03	forest_frac	27.59	0.7259	0.7236	21.25
317.00	HAI	237.59	de	-263.42	sand_frac	-53.96	0.7259	0.7236	15.82
283.50	HAI	245.93	de	-274.18	silt_frac	50.02	0.7237	0.7215	17.23
293.98	HAI	255.24	de	-264.65	ST	-33.14	0.7237	0.7214	16.23
262.86	HAI	272.01	de	-240.52	ST	-35.29	0.7207	0.7184	16.22
285.14	HAI	255.89	de	-244.48	sand_frac	-43.70	0.7206	0.7183	15.69
271.74	HAI	272.68	de	-243.37	high_prec_tim	-5.27	0.7202	0.7179	33.29
253.89	HAI	262.56	de	-251.52	silt_frac	47.96	0.7200	0.7177	17.38
249.56	HAI	272.60	sp	64.52	de	-265.32	0.7186	0.7163	15.93
254.10	HAI	260.40	sp	56.58	de	-259.95	0.7088	0.7064	15.52
294.19	HAI	245.62	de	-233.48	sand_frac	-75.97	0.7020	0.6995	15.85
248.58	HAI	257.57	de	-247.44	silt_frac	63.38	0.6967	0.6942	17.62
296.12	HAI	235.67	de	-235.96	sand_frac	-63.09	0.6957	0.6932	15.42

Figure G.3: The best iterations for the model with 4 independent variables.

constant	param1	coef1	param2	coef2	param3	coef3	param4	coef4	Rsquared	Rsquared adj	cond num
272.84	HAl	251.78	sp	63.14	de	-251.03	sand_frac	-65.27	0.7236	0.7205	16.43
203.60	HAl	276.37	sp	64.86	de	-228.33	forest_frac	27.86	0.7215	0.7184	22.58
231.42	HAl	261.70	sp	63.19	de	-263.21	silt_frac	61.04	0.7206	0.7175	18.56
276.90	HAl	257.94	sp	65.48	de	-256.78	sand_frac	-65.49	0.7201	0.7170	16.68
229.66	HAl	267.91	sp	64.49	de	-266.48	silt_frac	72.21	0.7189	0.7158	18.72
246.31	HAl	260.17	Sl	55.97	sp	61.91	de	-267.63	0.7178	0.7147	21.97
281.03	HAl	255.93	sp	63.70	de	-281.94	low_prec_tim	-3.47	0.7174	0.7143	43.45
269.68	HAl	266.12	sp	67.41	de	-258.64	sand_frac	-55.78	0.7168	0.7137	16.44
218.38	HAl	279.40	sp	65.05	de	-241.46	forest_frac	23.42	0.7159	0.7128	22.24
273.24	HAl	254.54	sp	60.78	de	-249.09	sand_frac	-66.28	0.7155	0.7124	16.44
224.05	HAl	264.83	sp	61.75	de	-259.98	silt_frac	76.69	0.7150	0.7119	18.39
213.77	HAl	285.57	sp	69.26	de	-241.75	forest_frac	22.28	0.7144	0.7113	22.26
234.10	HAl	274.75	sp	67.46	de	-268.15	silt_frac	50.13	0.7141	0.7110	18.52
286.45	HAl	260.94	sp	65.77	de	-287.39	low_prec_tim	-3.82	0.7140	0.7109	42.28
253.08	HAl	265.42	Sl	43.84	sp	63.06	de	-272.65	0.7132	0.7101	21.78
243.75	HAl	272.69	Sl	60.32	sp	67.07	de	-271.98	0.7129	0.7098	22.57
270.73	HAl	270.48	sp	67.76	de	-280.69	low_prec_tim	-2.29	0.7116	0.7084	42.75
212.61	HAl	276.66	sp	62.38	de	-233.18	forest_frac	23.27	0.7114	0.7082	22.12
272.84	HAl	251.78	sp	63.14	de	-251.03	sand_frac	-65.27	0.7236	0.7205	16.43
203.60	HAl	276.37	sp	64.86	de	-228.33	forest_frac	27.86	0.7215	0.7184	22.58

Figure G.4: The best iterations for the model with 5 independent variables.

constant	param1	coef1	param2	coef2	param3	coef3	param4	coef4	param5	coef5	rsquared	rsquared_adj	cond_num
230.27	HAI	278.12	sp	65.19	de	-223.53	sand_frac	-76.63	forest_frac	25.78	0.7541	0.7507	22.92
263.04	HAI	266.67	SI	62.25	sp	63.79	de	-262.84	sand_frac	-63.68	0.7516	0.7481	22.94
302.86	HAI	261.90	sp	65.55	de	-279.44	sand_frac	-63.19	low_prec_tim	-4.11	0.7514	0.7480	42.75
290.47	HAI	273.97	sp	61.09	de	-254.17	sand_frac	-88.19	clay_frac	-63.49	0.7511	0.7477	27.65
179.56	HAI	291.54	SI	111.23	sp	67.00	de	-236.48	forest_frac	30.76	0.7509	0.7475	27.89
153.24	HAI	294.97	SI	117.19	sp	71.21	de	-216.04	forest_frac	35.96	0.7353	0.7317	27.98
204.58	HAI	284.21	sp	68.73	de	-208.96	sand_frac	-61.29	forest_frac	29.06	0.7350	0.7314	22.89
171.56	HAI	292.62	sp	67.53	de	-223.36	silt_frac	53.85	forest_frac	26.05	0.7319	0.7282	24.37
243.49	HAI	269.18	SI	67.86	sp	65.29	de	-251.22	sand_frac	-50.20	0.7318	0.7281	22.84
273.25	HAI	278.53	sp	63.57	de	-242.80	sand_frac	-76.83	clay_frac	-70.04	0.7314	0.7277	27.92
254.48	HAI	257.78	SI	70.02	sp	64.16	de	-253.74	sand_frac	-54.67	0.7278	0.7241	23.02
286.55	HAI	268.78	sp	60.70	de	-243.92	sand_frac	-84.40	clay_frac	-78.64	0.7278	0.7241	27.85
241.39	HAI	266.53	sp	63.79	de	-229.69	sand_frac	-63.99	forest_frac	15.76	0.7266	0.7229	22.71
268.56	HAI	253.57	sp	65.96	de	-257.15	sand_frac	-62.53	high_prec_tim	3.07	0.7259	0.7221	34.84
218.22	HAI	266.45	SI	76.20	sp	65.16	de	-264.97	silt_frac	52.63	0.7258	0.7221	22.60

Figure G.5: The best iterations for the model with 6 independent variables.

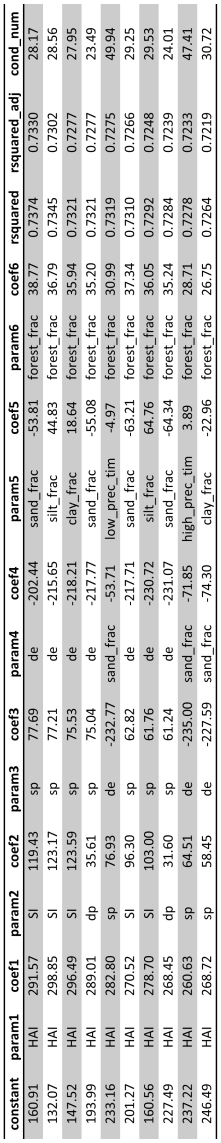

constant	param1	coef1	param2	coef2	param3	coef3	param4	coef4	param5	coef5	param6	coef6	rsquared	rsquared_adj	cond_num
160.91	HAI	291.57	SI	119.43	sp	77.69	de	-202.44	sand_frac	-53.81	forest_frac	38.77	0.7374	0.7330	28.17
132.07	HAI	298.85	SI	123.17	sp	77.21	de	-215.65	silt_frac	44.83	forest_frac	36.79	0.7345	0.7302	28.56
147.52	HAI	296.49	SI	123.59	sp	75.53	de	-218.21	clay_frac	18.64	forest_frac	35.94	0.7321	0.7277	27.95
193.99	HAI	289.01	dp	35.61	sp	75.04	de	-217.77	sand_frac	-55.08	forest_frac	35.20	0.7321	0.7277	23.49
233.16	HAI	282.80	sp	76.93	de	-232.77	sand_frac	-53.71	low_prec_tim	-4.97	forest_frac	30.99	0.7319	0.7275	49.94
201.27	HAI	270.52	SI	96.30	sp	62.82	de	-217.71	sand_frac	-63.21	forest_frac	37.34	0.7310	0.7266	29.25
160.56	HAI	278.70	SI	103.00	sp	61.76	de	-230.72	silt_frac	64.76	forest_frac	36.05	0.7292	0.7248	29.53
227.49	HAI	268.45	dp	31.60	sp	61.24	de	-231.07	sand_frac	-64.34	forest_frac	35.24	0.7284	0.7239	24.01
237.22	HAI	260.63	sp	64.51	de	-235.00	sand_frac	-71.85	high_prec_tim	3.89	forest_frac	28.71	0.7278	0.7233	47.41
246.49	HAI	268.72	sp	58.45	de	-227.59	sand_frac	-74.30	clay_frac	-22.96	forest_frac	26.75	0.7264	0.7219	30.72